Biological response to mesoscale eddies in the Algerian Basin

I. Taupier-Letage, I. Puillat, and C. Millot

Laboratoire d'Océanographie et Biogéochimie (LOB), CNRS UMR 6535, Université de la Méditerranée, Antenne de Toulon, La Seyne sur Mer, France

P. Raimbault

Laboratoire d'Océanographie et Biogéochimie (LOB), CNRS UMR 6535, Université de la Méditerranée, Campus de Luminy, Marseille, France

Received 1 November 1999; revised 14 March 2001; accepted 29 June 2001; published 1 August 2003.

[1] The Eddies and Leddies Interdisciplinary Study in the Algerian Basin (ELISA) experiment (1997–1998, MAST-3/MTP2/MATER program) was a multidisciplinary and multiplatform experiment designed to study the anticyclonic Algerian Eddies (AEs) generated by the instability of the Algerian Current and their influence on the general circulation and biological phenomena. This paper presents preliminary results of the data obtained over the four year-round cruises ELISA-1 to 4. Two AEs (called 96-1 and 97-1) were tracked with satellite images over their counterclockwise circuit in the eastern Algerian Basin, from the Algerian to the Sardinian slope, and then to the open sea. They have been sampled over different periods and positions. Associated biological response was analyzed considering the hydrodynamical structure and the distribution of chlorophyll and nitrate concentration in the upper 300 m. In summer both AEs (96-1 located along slope and 97-1 located offshore) corresponded to highly oligotrophic areas. The deep chlorophyll maximum was ~90–110 m, with concentrations up to ~1 mg m^{-3}, the nitrate concentrations were low down to ~250 m in the AEs' central zone. The downward entrainment of chlorophyll along isopycnals in the AEs' peripheral zone was well observed down to ~250 m. In spring the maximum integrated chlorophyll concentrations were found offshore, in 96-1, where the upper ~150 m were quasi-homogeneous. Lower integrated chlorophyll concentrations were found inshore in 97-1, which was embedded in an Algerian Current meander and remained stratified throughout wintertime. AEs generate secondary phenomena such as small-scale cyclonic shear eddies, where the highest chlorophyll concentrations (~4 mg m^{-3}) were found. We show that through the AEs it generates, the Algerian Current can be responsible for producing areas in the coastal zone that are at least as oligotrophic as the eastern Mediterranean and, alternately, for productive areas offshore. As AEs generally follow a counterclockwise circuit in the Algerian Basin, it is inferred that they play an important role in the redistribution of matter on a basin scale. However, the biological response associated with AEs varies according to their history, a combination of trajectory, location, and season, in ways that are not yet clear. *INDEX TERMS:* 4223 Oceanography: General: Descriptive and regional oceanography; 4520 Oceanography: Physical: Eddies and mesoscale processes; 4845 Oceanography: Biological and Chemical: Nutrients and nutrient cycling; 4855 Oceanography: Biological and Chemical: Plankton; 4275 Oceanography: General: Remote sensing and electromagnetic processes (0689); *KEYWORDS:* Mediterranean, Algerian Current, mesoscale eddies, chlorophyll, nitrate, ELISA/MATER

Citation: Taupier-Letage, I., I. Puillat, C. Millot, and P. Raimbault, Biological response to mesoscale eddies in the Algerian Basin, *J. Geophys. Res.*, *108*(C8), 3245, doi:10.1029/1999JC000117, 2003.

1. Introduction

[2] Water from the Atlantic enters the Mediterranean Sea at Gibraltar mainly to compensate for water lost by evaporation. Because of mixing, it rapidly becomes Atlantic Water (AW), which constitutes the surface circulation in the western Mediterranean (Figure 1, see *Millot* [1999] and *Send et al.* [1999] for a review). AW flows along the Algerian slope, forming the Algerian Current. This current is unstable, meanders and generates mesoscale eddies [e.g., *Millot*, 1985; *Font et al.*, 1998]. A typical Algerian Current instability can be described as a meander (AW layer, ~200 m thick) embedding a (coastal) anticyclonic eddy, associated with an upwelling

0148-0227/03/1999JC000117

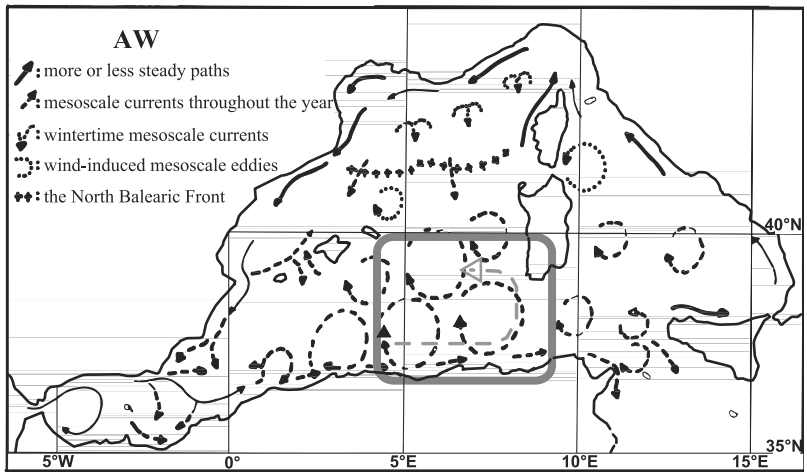

Figure 1. The general circulation of the Atlantic Water (AW) in the western Mediterranean [adapted from *Millot*, 1999]. The dashed gray arrow represents the general counterclockwise circuit of AEs. The gray rectangle indicates the ELISA area.

cell on its southwestern side, and often with a short-lived shallow cyclonic circulation on the meander crest [e.g., *Obaton et al.*, 2000; *Moran et al.*, 2001]. Only the anticyclonic eddies develop (hereafter Algerian Eddies, AEs; see Figure 2 for illustration), so as to reach diameters of 50–100 km (up to ~280 km), and vertical extents of thousands of meters down to the bottom (~2800 m [*Ruiz et al.*, 2002; *Millot and Taupier-Letage*, 2003]). AEs propagate downstream along slope at a few km/day (e.g., 97-1 between Figures 2a and 2e), and are likely to detach from the coast after pinching off from the Algerian Current when approaching the Channel of Sardinia, because of the shallowing and narrowing bathymetry. AEs then skirt the Sardinian slope (e.g., 97-1 on Figure 2g) where they interact with the Levantine Intermediate Water (LIW) vein [*Millot*, 1987; *Millot and Taupier-Letage*, 2003], and propagate westward offshore in the central part of the basin (open sea AE). The resulting trajectory is a counterclockwise circuit in the eastern Algerian Basin [*Fuda et al.*, 2000]. This circuit can be closed, as some AEs come back in the Algerian coastal zone, and can include several loops, up to three loops for 96-1 [*Puillat et al.*, 2002]. The lifetime of most AEs is of the order of several months to 1 year [e.g., *Millot et al.*, 1997], and one AE (96-1, see section 1.3) has been tracked for nearly 3 years [*Puillat et al.*, 2002]. When located along the Algerian slope, AEs in turn can interact with the Algerian Current (as 97-1, relayed by 96-1, on Figure 2e) and dramatically alter its circulation [e.g., *Millot*, 1991; *Benzohra and Millot*, 1995a]. AEs often generate secondary phenomena, such as small cyclonic shear eddies (~20–30 km) and filaments [*Taupier-Letage and Millot*, 1988].

[3] This dynamical mesoscale activity modulates the biological activity, as shown by the close correlation between thermal and ocean color satellite signatures [*Taupier-Letage*, 1988; *Arnone and La Violette*, 1986; *Arnone et al.*, 1990]. This implies that the biological activity is also affected by large spatial and temporal variability on the mesoscale [e.g., *Robinson*, 1983; *Morel and André*, 1991]. This can lead, locally and episodically, to unexpectedly high chlorophyll or primary production values for the Mediterranean [*Lohrenz et al.*, 1988a, 1988b; *Arnone et al.*, 1990; *Martinez et al.*, 1990; *Raimbault et al.*, 1993]. To accurately describe the biological activity in such areas, it is therefore important to design a mesoscale-dedicated sampling strategy [e.g., *Aiken et al.*, 1993]. This implies multidisciplinary and multiplatform experiments, with data collection at small sampling intervals (few km) within a short time (a few days), preferably over long periods (~1 year) and over large areas (up to basin scale). Moreover, efficient shipboard sampling requires one to be aware of the mesoscale field. This can be achieved with the (near) real time reception of satellite images (easily accessed nowadays) on board, as satellite observations of mesoscale phenomena are well correlated to in situ ones in the Algerian Basin [*Millot et al.*, 1994, 1997; *Fuda et al.*, 2000]. Given these constraints, such experiments are few. Between 1986 and 1987, the Mediprod-5 experiment [*Mediprod-5 Group*, 1990] explored the western part of the Algerian Basin on a mesoscale.

Figure 2. (opposite) Mesoscale location and sampling sites during the ELISA cruises (only the best time coherent subsets of satellite and in situ observations are presented). Pluses are CTD transects discussed in text, identified by their end station numbers. Solid triangles are moorings. Temperature on NOAA/AVHRR images increases from blue to red. Arrows are shipboard ADCP currents in the 16–50-m layer. (a) ELISA-1 CTD transects over NOAA/AVHRR image of 28 July 1997. (b) ADCP currents from 24 July to 2 August 1997 over NOAA/AVHRR image of 27 July 1997. (c) ELISA-2 CTD transect over NOAA/AVHRR image of 19 October 1997. d) NOAA/AVHRR image of 27 October 1997. (e) ELISA-3 CTD transects over NOAA/AVHRR image of 27 March 1998. (f) ADCP currents from 26 to 28 March 1998, over NOAA/AVHRR image of 27 March 1998. (g) ELISA-4 CTD transect over NOAA/AVHRR image of 6 July 1998. (h) ADCP from 1 to 6 July 1998 over NOAA/AVHRR image of 6 July 1998. See color version of this figure at back of this issue.

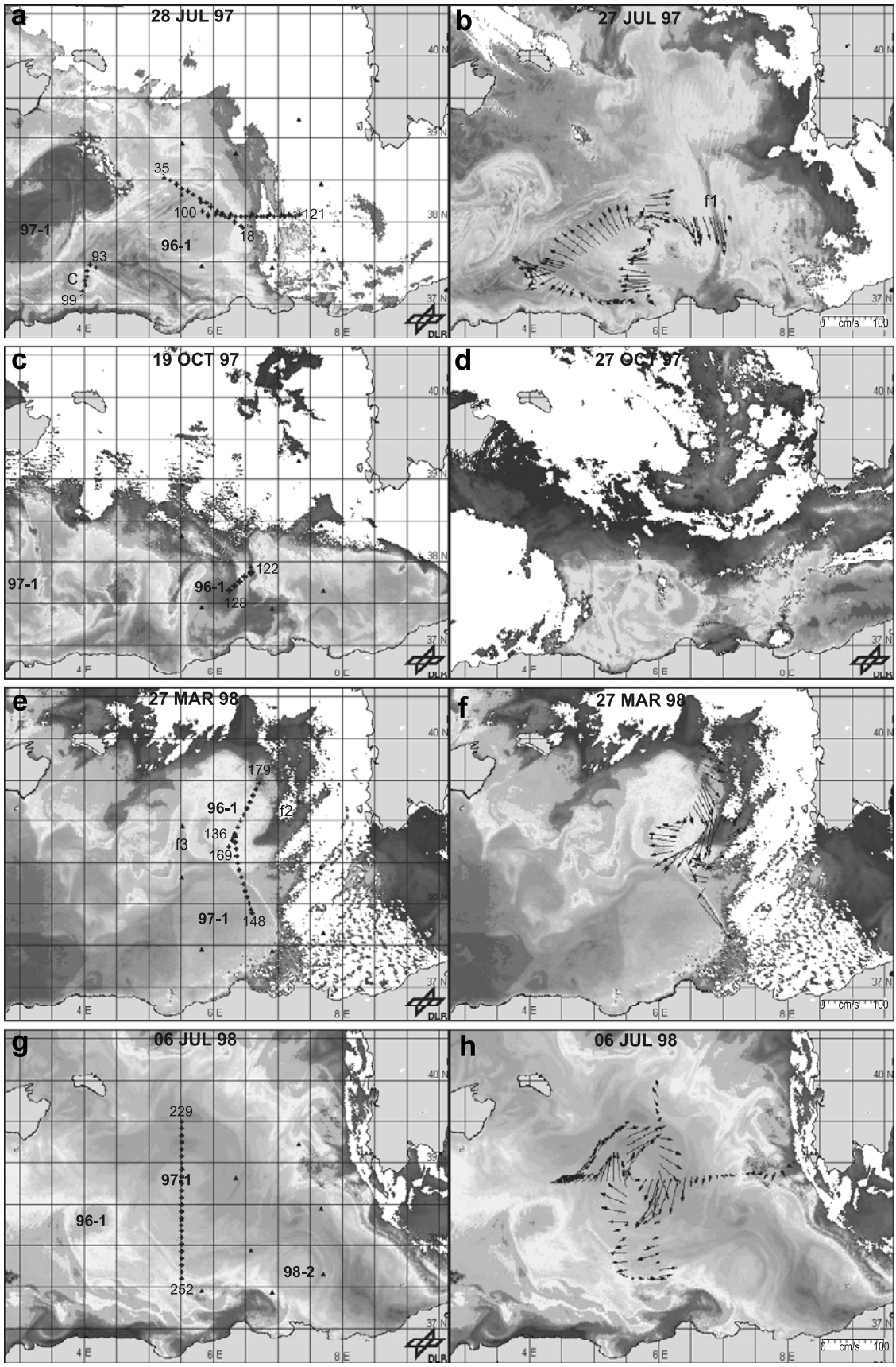
a
28 JUL 97
35
100
121
18
97-1
96-1
93
C
99
b
27 JUL 97
f1
0 cm/s 100
c
19 OCT 97
122
97-1
96-1
128
d
27 OCT 97
e
27 MAR 98
179
96-1
f2
f3
136
169
97-1
148
f
27 MAR 98
0 cm/s 100
g
06 JUL 98
229
97-1
96-1
98-2
252
h
06 JUL 98
0 cm/s 100

Table 1. Summary of the Cruises and Operations at Sea During the ELISA Experiment

Name	Dates	R/V	Operations
ELISA-1	1 July to 8 Aug. 1997	*Le Suroît*	deployment of moorings 1–8 and drifters, CTD, XBT, SEASOAR, LHPR, EK500, biology, biogeochemistry
ELISA-1.33	5–8 Sept. 1997	*Georges Petit*	recovery of mooring 6, XBT
ELISA-1.66	3–7 Oct. 1997	*BI "Green Peace"*	recovery of mooring 8
ELISA-2	20–29 Oct. 1997	*Tethys-2*	deployment of moorings 6, 8, 9 and CTD
ELISA-2.5	18 Feb. to 9 March 1998	*Georges Petit*	recovery and deployment of six moorings to replace defective acoustic release rings.
ELISA-3	19–30 March 1998	*Le Suroît*	moorings, CTD, XBT
ELISA-4	22 June to 8 July 1998	*Le Suroît*	moorings recovery, CTD, XBT

Results confirmed the high variability of chlorophyll and nutrient distribution, in relation to mesoscale dynamical structures: the lowest chlorophyll concentrations were found in the central part of an open sea AE, the highest (>9 mg m^{-3}) in a small-scale cyclonic shear eddy [*Taupier-Letage*, 1988; *Raimbault et al.*, 1988a, 1988b, 1990a]. In the westernmost part of the basin, biological enhancement related to an Algerian Current instability was observed, especially in its shallow and transient cyclonic circulation [*Moran et al.*, 2001]. However, most investigations focused on the biological enhancement at the outer edge of the Algerian Current between 0 and ~3°E, as it often delimits a front [*Lohrenz et al.*, 1988b; *Raimbault et al.*, 1993]. On average, the dynamical activity of the Algerian Current is well marked by a more productive coastal zone, as shown by satellite-derived chlorophyll concentrations and primary production maps [e.g., *Antoine et al.*, 1995]. It is also marked, in a coastal zone ~50 km wide, by an intermediate (~300–600 m) maximum of nutrients (nitrate >9.0 μM, phosphate >4.0 μM) indicating the occurrence of intense remineralization [*Raimbault et al.*, 1990b].

[4] The need for another experiment was prompted by the high mesoscale variability found and the limited observations of the seasonal variability, which prevented generalization from the few sampled AEs. The aim of this paper is to present the preliminary results obtained during the 1-year ELISA experiment [*ELISA Group*, 1998] (http://www.com.univ-mrs.fr/ELISA) on the biological response to AEs, represented here by the distribution of chlorophyll and nitrate concentration. First we present the ELISA experiment, the data sets and the trajectories of the AEs encountered (section 2). Then we describe the biological response associated with these eddies (section 3), and the secondary phenomena they induce (section 4). We discuss the consequences on a mesoscale and seasonal scale (section 5) and finally put forward hypotheses for consequences on a basin scale (section 6).

2. ELISA Experiment

[5] ELISA stands for Eddies and Leddies Interdisciplinary Study in the Algerian basin (Leddies are hypothetical eddies which could be created in theory by the instability of the LIW vein as it goes round the southwest corner of Sardinia [*Millot et al.*, 1997]). This experiment was part of the Mass Transfer and Ecosystem Response (MATER) MAST3-MTP2 European program, and involved 44 physicists, biologists and geochemists from 8 countries (http://www.com.univ-mrs.fr/ELISA). The major aims of ELISA were to study: (1) the general circulation of the water masses, (2) the origin, structure and trajectories of AEs, and (3) the biological response associated with mesoscale dynamical phenomena, and (4) the biological consequences of the mesoscale dynamics for the functioning of the Algerian Basin. Work at sea was carried out in the eastern part of the Algerian Basin from July 1997 to July 1998. It involved four main cruises (Table 1), the 1-year deployment of a mooring network (Figure 3) and of 15 subsurface Lagrangian drifters, and the continuous monitoring of the area by satellite thermal NOAA/AVHRR imagery analysis. The four cruises ELISA-1 to 4 were scheduled year-round to carry out mooring operations (including the periodic maintenance of bio-optical moored sensors to avoid biofouling problems) and sampling (Figure 4).

2.1. Data Sets

2.1.1. Satellite Imagery

[6] The situation on a basin scale was first analyzed using the Mediterranean daily composited NOAA/AVHRR SST

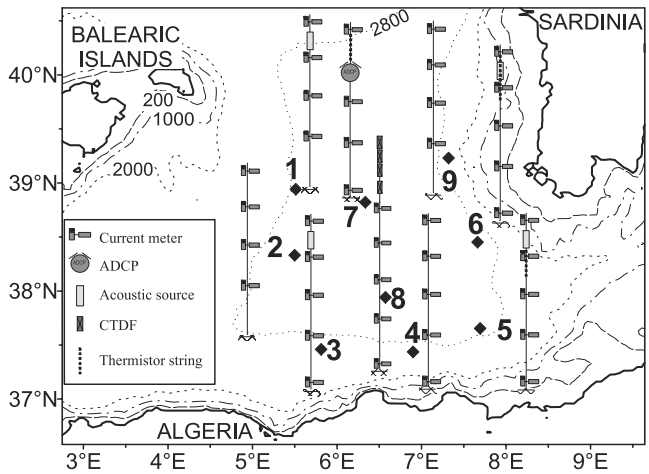

Figure 3. The ELISA experiment area. Bathymetry is in meters. ELISA moorings positions (solid diamonds 1–9) and schematics.

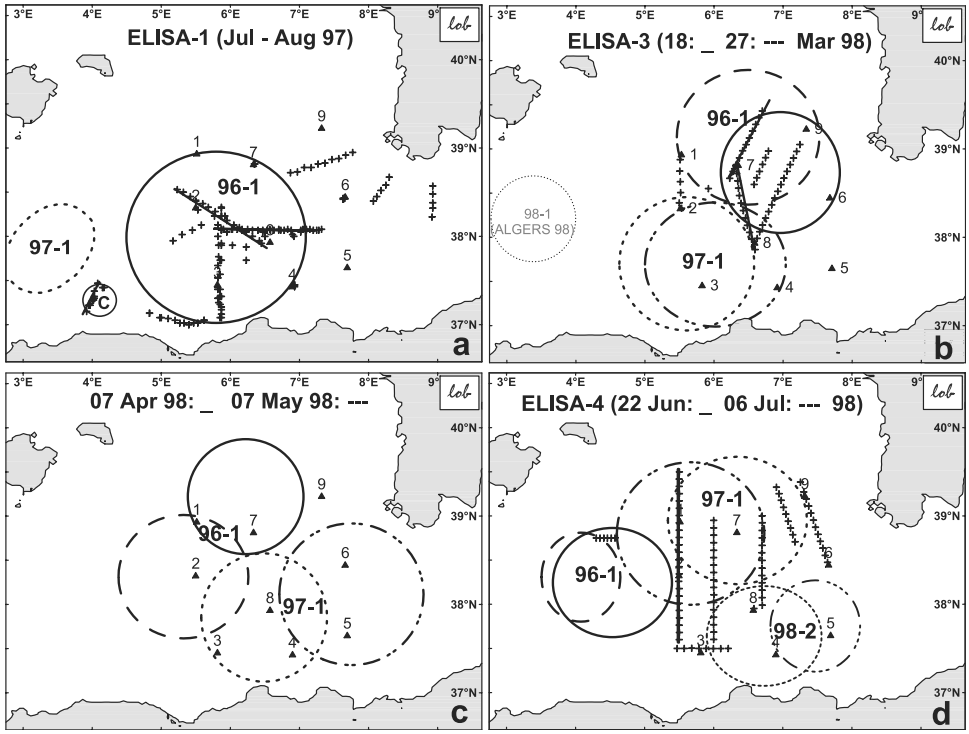

Figure 4. AEs' schematic positions and CTD sampling in (a) summer 1997, (b)–(c) spring 1998, and (d) summer 1998. See text for eddy identification; positions and diameters of AEs as estimated from their NOAA/AVHRR signatures on indicated dates. Pluses are CTD stations; thick lines are transects discussed in paper; and triangles 1–9 are mooring positions.

(Sea Surface Temperature) images of the ISIS database (http://isis.dlr.de), starting mid-1996. In order to get adequate information for tracking mesoscale features using thermal signatures [*Taupier-Letage et al.*, 1998], the German Aerospace Centre (DFD/DLR) generated AVHRR channel 4 images (relative temperatures) of all passes on the eastern Algerian Basin in near real time. These files were retrieved *via* ftp, including from the ship while at sea. Over 1000 such images (hereafter generically called SST) have been analyzed. Images are color-coded in order to enhance thermal contrast: as a consequence there is no standard temperature-to-color scale.

2.1.2. CTD Casts

[7] The shipboard CTDs were Seabird SBE 911 +, calibrated within a few months at most from the cruises. Accuracy and precision for potential temperature, salinity and potential density are known better than ±0.1%. For each cruise, the CTD was fitted at least with an in situ Chelsea Aquatracka MK3 fluorometer, a SeaTech 25 cm path length transmissometer at 660 nm, and a Seabird dissolved oxygen probe. Casts were typically made to 1000 m, and the reference level for the computation of the geostrophic current was 1000 dbar. However, casts down to 200 m were sometimes interleaved to improve spatial resolution without impacting time. Alternately, some casts were extended down to 2000 m or down to the bottom when prompted by hydrological peculiarities, as well as to check the vertical extent of AEs. Acquisition rate for all sensors was 24 scans s^{-1}. Data were processed using Seabird/Seasoft software, and averaged over 1 m bins. Transects, presented only in the upper 300 m, are identified by their end station numbers. A Seabird 12l 12-bottle carrousel was used for water samples.

2.1.3. Chlorophyll Concentrations

[8] Chlorophyll *a* concentrations were estimated fluorometrically after extraction of pigment in methanol as described by *Herbland et al.* [1985] and modified by *Raimbault et al.* [1988a], a rapid method especially adapted to dense mesoscale sampling. Water samples of 250 mL were filtered using Whatman GF/F fiberglass filters (25 mm) under low vacuum pressure ($\leq$100 mm Hg). Filters were placed in a glass tube with 5 mL of pure methanol and kept in the dark at $\sim$4°C for $\sim$30 min. The fluorescence of extracts was measured with a Turner Designs fluorometer before acidification, for chlorophyll concentration = chlorophyll *a* + phaeophytin *a* concentration, and after, for chlorophyll *a* and phaeophytin *a* respective concentrations. We used the former extracted chlorophyll to calibrate the in situ fluorometer signal. Indeed, the best vertical representation of the chlorophyll profile is given by the CTD downcasts, as the discrete water samples cannot assess correctly the amplitude of chlorophyll maxima, or its vertical variability. Also, during upcasts the stratification is disturbed by the CTD before water samples are taken, which results in severe underestimation of peaks, if sampled at all. For each cruise, the upcast bottle fluorescence was plotted *vs.* the corresponding extracted chlorophyll concentrations (abbreviated hereafter to "ec"). The derived relation was then applied to the downcast fluorescence profile to yield instrumentally and seasonally comparable chloro-

phyll concentrations, and to compute reliable integrated chlorophyll concentrations. These concentrations are used throughout the text, and sometimes backed up by the ec ones.

2.1.4. Nutrients

[9] During ELISA-1 nutrients were analyzed immediately on board (third leg only, from stations 78 to 121). During ELISA-2 no sample was taken. During ELISA-3 nutrient samples were frozen for eventual analysis in the laboratory, but it seems that a preservation problem occurred and concentrations were not all reliable. During ELISA-4 samples were collected in 25 mL polyethylene flasks and immediately poisoned with $HgCl_2$ (final concentration of 20 $\mu g\ mL^{-1}$) according to *Kirkwood* [1992]. Samples were then stored in the dark at $\sim 5°C$ until processing in the laboratory. Nitrate concentrations were determined on a Technicon AutoAnalyser according to *Tréguer and Le Corre* [1975]. Concentrations of nitrite and phosphate were also determined (as well as ammonium during ELISA-1), but are not addressed here.

2.2. Strategy

[10] As the mesoscale was a focal point of ELISA, an adaptable strategy was implemented. First the AEs were continuously tracked with SST images. While at sea, the images were sent in near real time to the ship. Once the structure to sample was determined, the sampling scheme was refined considering currents from shipboard ADCP and indications from thermosalinograph, as well as from XBT sections. Besides rapid reconnaissance, XBTs were also used to extend CTD transects in less critical areas in order to save time, and more generally during transits in the Algerian Basin. A mean sampling interval of 5 nautical miles ($\sim$9 km) was used, sometimes reduced to 3 miles ($\sim$5 km). Care was taken to complete transects across structures within a few days. The main interdisciplinary effort was made during the ELISA-1 cruise. It was divided into three legs to put the moorings in place, to make rapid synoptic surveys of AEs with XBTs, CTD, and Seasoar (tow-yo), and, last, to allow for time-demanding biological and biogeochemical sampling, respectively. In addition to time-limited shipboard sampling, efforts were made to obtain the mesoscale structures description on a longer term. A network of nine mooring lines $\sim$50 km spaced (Figure 3) provided 1-year-long time series. More than 40 current meters sampled in the main water masses down to the bottom. Mooring 8 was equipped with four autonomous CTDs fitted with fluorometers (CTDFs) at $\sim$40, 50, 60, and 80 m (nominal depths), and mooring 7 was equipped with an RDI 75 kHz ADCP sampling the upper 500 m.

2.3. Trajectories of AEs During the ELISA Experiment

[11] Two main AEs, called 96-1 and 97-1, dominated the ELISA eddy field (Figure 4). Their history and trajectory are detailed by *Puillat et al.* [2002].

[12] From June to November 1997, 96-1 remained centered on $\sim 6°E$. Although 96-1 was close to the slope (Figure 4a), it was at least 15 months old, and had already completed one counterclockwise loop in the basin. 96-1 (diameter $\sim$180 km) was intensively sampled during ELISA-1. The shear between 96-1 and coastline breaks sporadically generated small cyclonic shear eddies, one of which (C) was spotted on the SST images (Figures 2a–2b) and sampled. The second AE, 97-1 ($\sim$120 km diameter), had been generated near $\sim 0°$ by late March 1997 and had been propagating along slope. 97-1 was thus a coastal eddy still embedded in an Algerian Current meander. By early July it was next to 96-1 (Figures 2a–2b). It altered the eastward along-slope propagation of AW, which was then deflected offshore, skirting 97-1 and 96-1 successively. Complex eddy interactions led to secondary phenomena such as filaments and dramatic changes in shape and/or diameters for both 96-1 and 97-1.

[13] By October 1997 (Figures 2c–2d), the diameter of 96-1 was reduced to $\sim$80 km. Sampling (ELISA-2) of 96-1 was limited to its NE part. By December 1997 both 96-1 and 97-1 resumed their counterclockwise trajectory.

[14] By March 1998 (Figure 4b and Figures 2e–2f), 96-1 was offshore propagating westward, while 97-1 was propagating eastward along the Algerian slope. An important shear zone was created in between. Sampling (ELISA-3) mainly focused on 96-1, reaching the NE border of 97-1. AE 96-1 went over mooring 7 in late March (Figure 4c).

[15] By June 1998 (Figure 4d and Figures 2g–2h), 97-1 was also offshore. Interactions between the Algerian Current, 98-2 and 97-1 (and 96-1 to a lesser extent) notably altered the eastward along-slope AW path. Sampling (ELISA-4) mainly focused on 97-1.

3. AEs' Biological Response

[16] As only a limited amount of data is presented here, it must be kept in mind that the analysis actually relies upon a vast database, including in particular $\sim$1000 SST images, $\sim$300 CTD casts over 269 stations, $\sim$350 XBT casts, $\sim$1400 determinations of nutrients, $\sim$40 current meters, and 4 CTDF 1-year-long time series (analyses are still ongoing).

3.1. AE 96-1

3.1.1. Summer (ELISA-1) and Autumn (ELISA-2) 1997 Conditions

[17] AE 96-1 did not propagate during summertime, so that the images presented on Figures 2a–2b are representative of all transects (made within 18 days). Its shape varied however, and its diameter ranged from $\sim$180 to $\sim$250 km. Associated maximum currents were $\sim$50 cm s^{-1}, up to 80 cm s^{-1} (Figure 2b and Figure 5a). These maxima lay subsurface ($\sim$50 to 100–150 m): there was a marked discontinuity at $\sim$50 m. The transect 18–35 along a SE-NW diameter (completed on 14–15 July, Figure 6) was representative of the general features of 96-1. Edges were not crossed, as indicated at transect extremities by geostrophic current $\sim$40 cm s^{-1} and sloping isolines. The thermocline (Figure 6a) was well marked in the central zone (stations 30–26 at $\sim$25 m) at 20–30 m, and weakened toward the edges. Hydrological sections displayed the classical trough of anticyclonic eddies, isolines being depressed by $\sim$150 m in the center. Isotherms and isopycnals (Figure 6c) were doming ($\sim$25 m) in the upper $\sim$75 m, a feature already observed by *Benzohra and Millot* [1995b]. AE 96-1 was characterized by a weakly stratified layer approximately 100-m thick in the central zone, between 50 and 150 m: temperatures were confined to 15.0°–16.0°C,

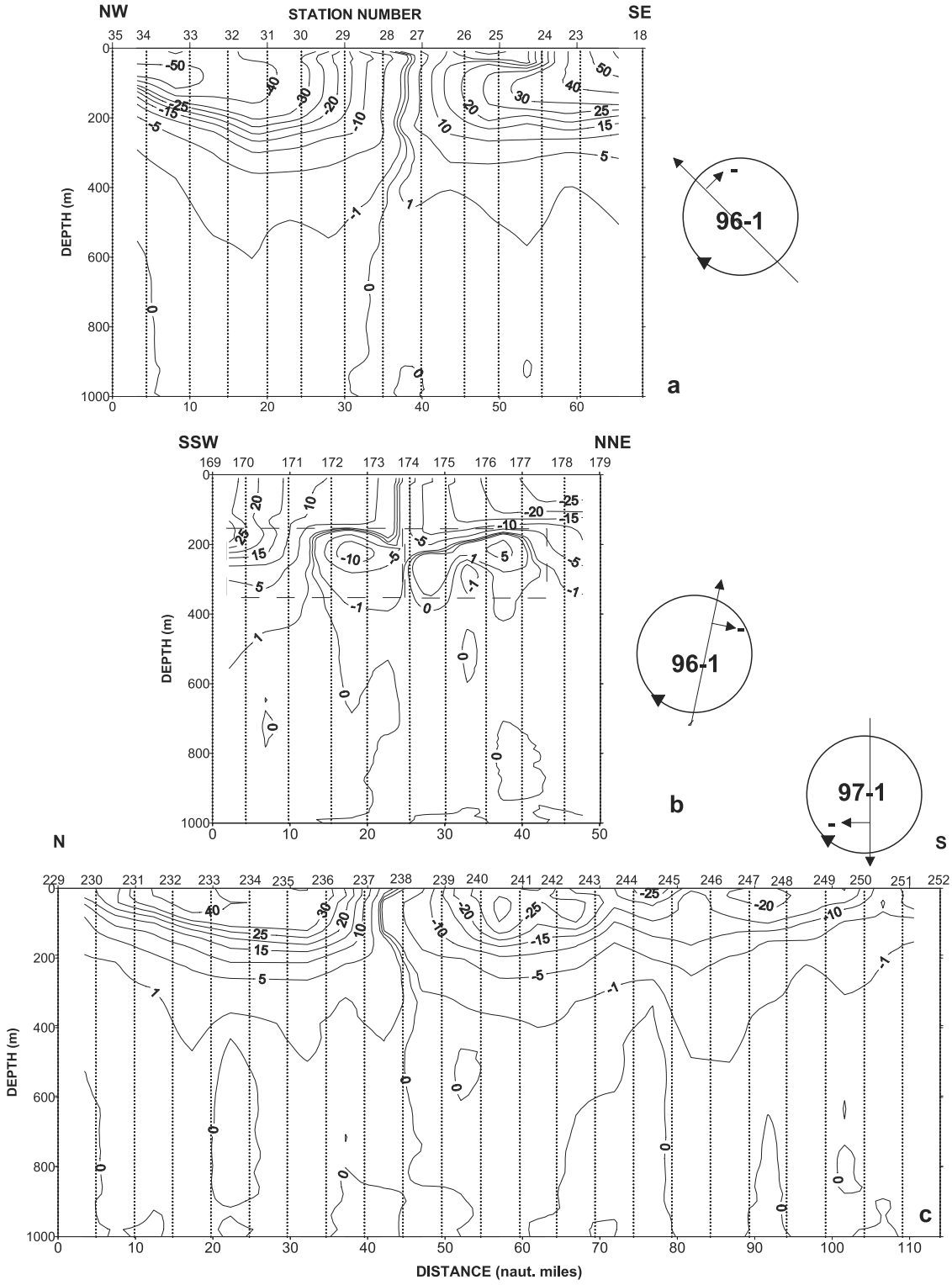

Figure 5. Geostrophic current (cm s^{-1}) sections (a) across 96-1 during summer 1997 (ELISA-1) and (b) spring 1998 (ELISA-3) and (c) across 97-1 during summer 1998 (ELISA-4). Orientation is given by respective schema.

salinities were confined to 37.00–37.10 (Figure 6b), and potential densities were confined to 27.20–27.60. Salinities lower than 37.00 (minimum 36.80) were found in patches, down to ~80 m. When plotting all the CTD profiles (not shown; see distribution on Figure 4a), minimum salinities (i.e., most recent/less mixed AW) were strikingly all inside 96-1, between ~40 and 60 m. Chlorophyll distribution (Figure 6c) was relatively symmetrical at eddy scale. There was no significant chlorophyll concentration in the upper ~30 m. The central zone displayed a deep chlorophyll

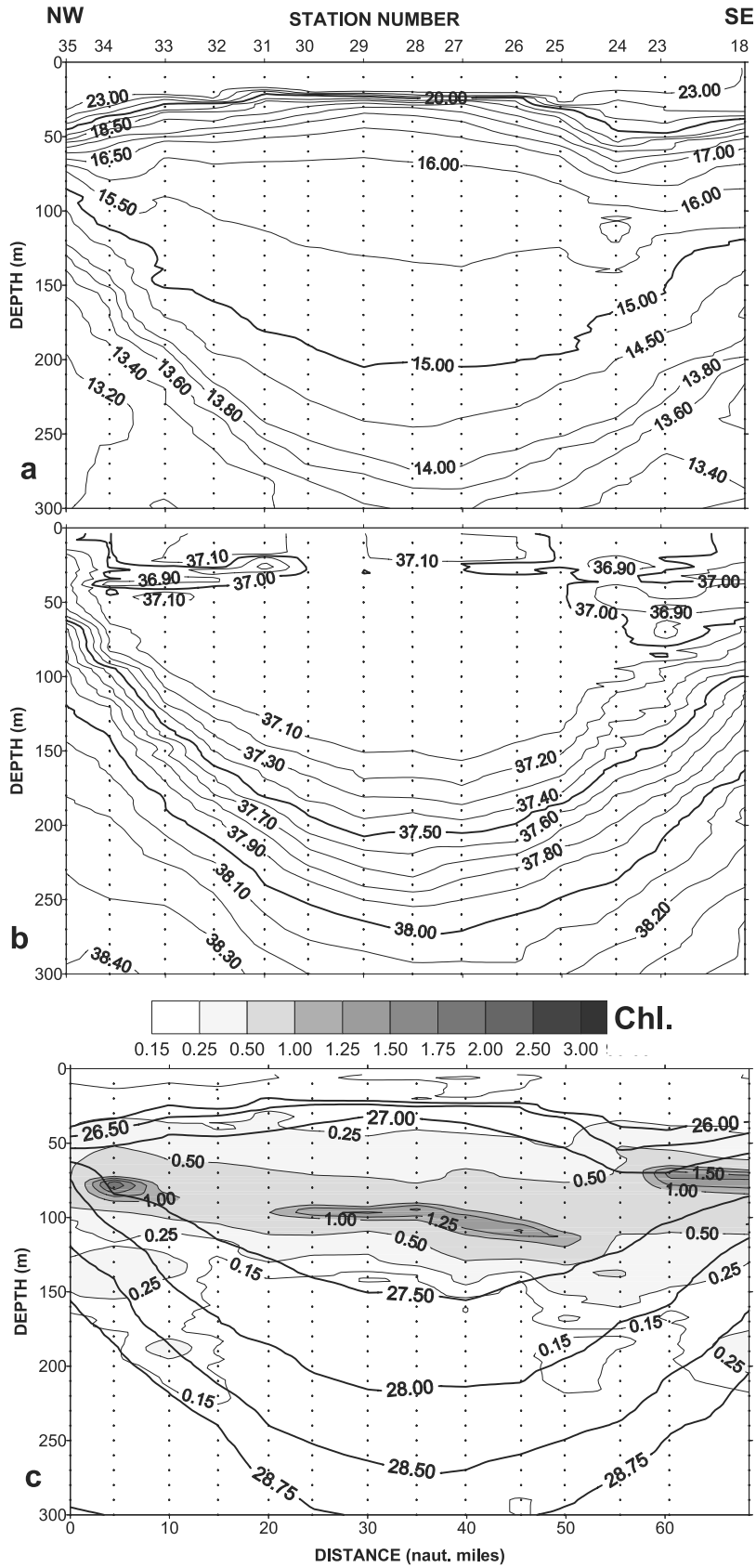

Figure 6. Transect 18–35 inside 96-1 (summer 1997): (a) potential temperature (°C), (b) salinity, and (c) chlorophyll concentration (mg m^{-3}) and potential density (thick solid line).

maximum (DCM), slightly deeper than in the peripheral zone. Maxima reached ~1.5 mg m^{-3} at stations 26, 28, and 29 at 100–110 m. In the peripheral zone maxima reached ~2.0 mg m^{-3} at station 34 and ~1.6 mg m^{-3} at station 23 at 70–80 m. Finally, significant chlorophyll concentrations were observed at ~200 m along the 28.50–28.75 isopycnals, at station 34 and station 18 (ec: 0.3 mg m^{-3} at 190 m). No nutrients were available for this transect.

[18] The transect 100–121 (Figure 7) across the eastern part of 96-1 was completed within 4 days (30 July to 2 August). The edge was marked at the surface in the vicinity of stations 116–119 by a sharp drop of the ADCP current speed (Figure 2b), as well as of the geostrophic current (not shown). A sharp salinity front in the vicinity of station 116 (Figure 7b) also marked the peripheral zone in the upper layer, where surface salinities were >37.60, and the 38.00 isohaline shoaled at ~70 m. Isohalines and isopycnals (Figure 7c) slopes were negligible from station 116 eastward but only in the upper ~100 m. This indicates that the deeper structure was wider. The center of 96-1 was located a few miles west of station 100. This is in agreement with the flat isolines at 100 m and the 28.00 isopycnal immersion (~210 m), as observed in the center of the 18–35 transect. Surface temperature increased to ~25.0°C (~23.5°C for 18–35, Figure 6a), and the thermocline was deeper by ~10 m. The ~100-m-thick central homogenous layer was well marked. The thin subsurface layer of lower salinity (<37.00) was quasi continuous (stations 100–113). The upper ~50 m were chlorophyll-depleted over the whole transect (Figure 7c). In the central zone the DCM lay between 100 and 110 m with maximum concentrations ~0.8 mg m^{-3}. The DCM slowly rose from ~100 m at station 106 to ~80 m at station 114 (maximum ~0.8–1.0 mg m^{-3}) toward the peripheral zone. In the vicinity of station 115 the 0.75 mg m^{-3} isopleth was interrupted. Below the DCM the chlorophyll signature progressively subsided centerward, from station 117 to station 113, following the 28.50–28.75 isopycnals down to ~200 m. Outside 96-1 the DCM did not appear significantly different from that in the 96-1 central zone. The nitrate-depleted upper layer (the 0.1-μM isopleth represents the detection limit) was ~60 m thick (Figure 7d) over the whole transect, slightly thicker in the 96-1 central zone and in the vicinity of station 114. The nutricline, represented by the 0.5-μM isopleth, was relatively horizontal too. Below, however, the nitrate distribution markedly differed in the central and peripheral zones. In the central zone of 96-1 (stations 100–107), concentrations were weak, ranging from ~1.0 to 2.5 μM from ~100 to 250 m. Concentrations were less than 7.0 μM at 300 m. From station 110 to 112 there was a marked nitrate gradient strengthening eastward, ending up at station 121 with concentrations of ~2.5 μM at ~100 m. Within 96-1 (other transects not shown) the isohaline 38.00 roughly corresponded to nitrate concentrations between 2.0 and 3.0 μM. In the peripheral zone this was no longer true, as the 38.00 isohaline was well above the 2.0–3.0 μM isopleth. Note that in the peripheral zone nitrate concentrations rapidly increased with depth: at station 121 the concentration reached ~9.0 μM at 300 m.

[19] The autumn transect in the NE peripheral zone of 96-1 (Figure 8) displayed similar features: a central homogeneous layer and a subsurface lower-salinity layer

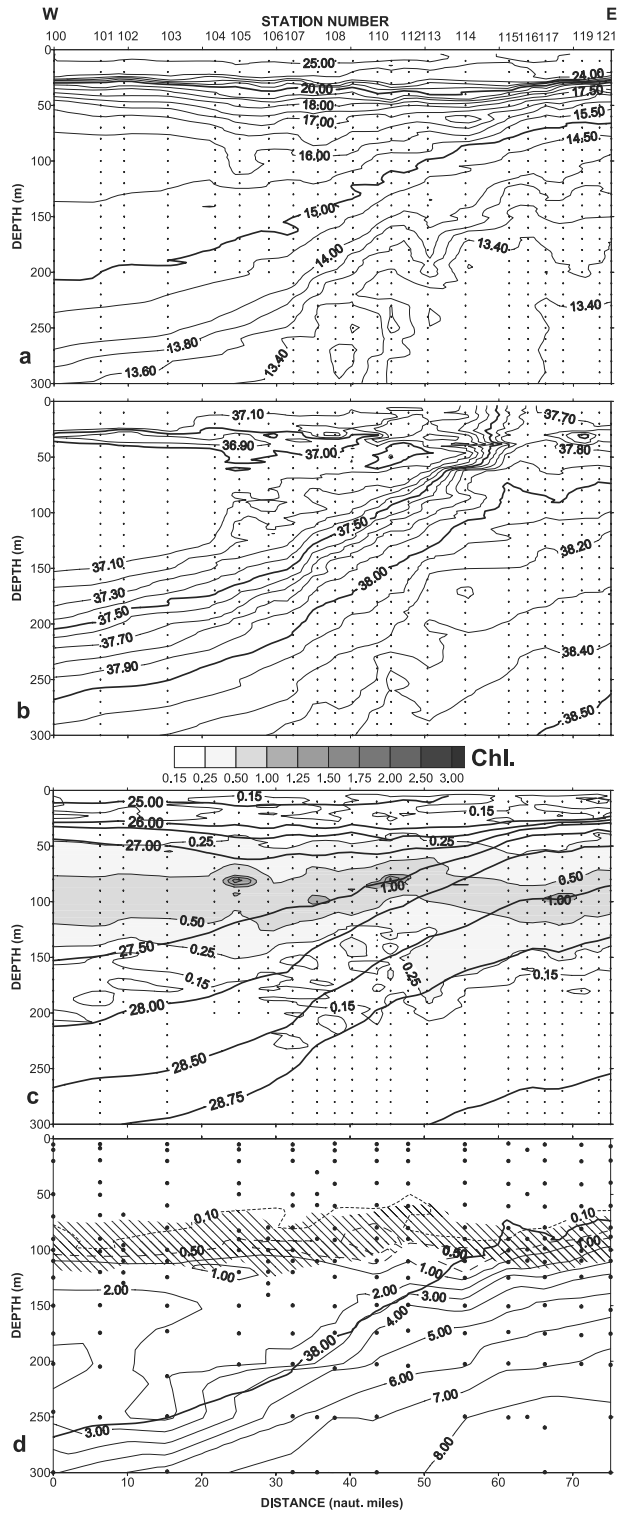

Figure 7. Transect 100–121 in 96-1 eastern half (summer 1997): (a) potential temperature (°C), (b) salinity, (c) chlorophyll concentration (mg m^{-3}) and potential density (thick solid line), and (d) nitrate concentration (μM); isohaline 38.00 (thick solid line), and chlorophyll >0.5 mg m^{-3} (cross-hatched).

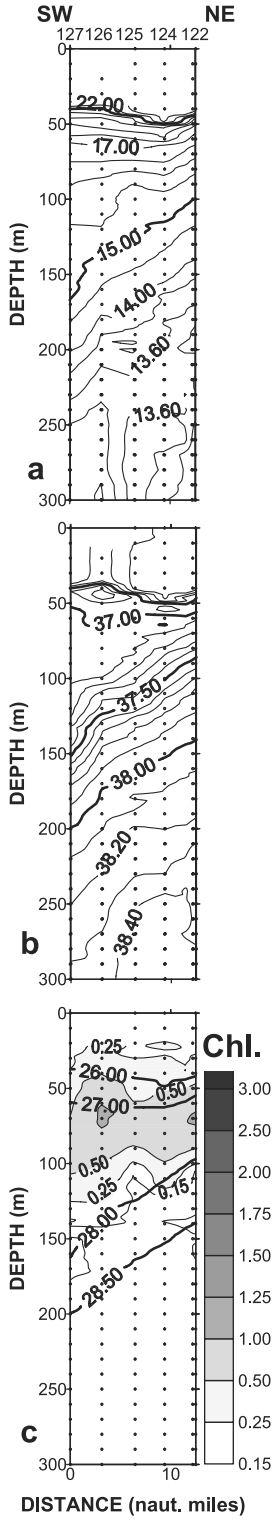

Figure 8. Transect 122–127 in the NE of 96-1 (fall 1997): (a) potential temperature (°C), (b) salinity, and (c) chlorophyll concentration (mg m^{-3}) and potential density (thick solid line).

(Figure 8b). Seasonal evolution however was marked by thermocline deepening (~50 m, Figure 8a) and mixed layer homogenization. The DCM ranged between 50 and 100 m, maxima hardly reached 1 mg m^{-3} (Figure 8c).

3.1.2. Spring 1998 Conditions (ELISA-3)

[20] AE 96-1 was offshore, propagating northwestward (Figures 4b–4c). The transect 169–179 (Figure 9) was completed on 28 March, ~36 hours after a ~2-day strong wind event. It cut 96-1 slightly east of its center (Figures 2e–2f), located between stations 173 and 174. Diameter estimates ranged from 130 to 160 km. Its structure had become complex, and was organized in three parts (Figure 5b): the main one was the upper layer (~180–200 m thick) along the whole transect length, overlaying two secondary cells between ~200–300 m (stations 170–173 and 175–179, respectively, identified by dashed boxes), which were in anticyclonic rotation on themselves. In the 96-1 upper layer the current was maximum (~25 cm s^{-1}) in the peripheral zone, and homogeneously weak (~0–10 cm s^{-1}) in the central one. The 96-1 upper central zone corresponded to a well-mixed layer: at station 174 the temperature (Figure 9a) only varied from 15.49°C at ~10 m to 15.46°C at ~150 m, and individualized an AW thermostad. In the same way the salinity was ~37.07 from the surface down to ~130 m (Figure 9b). On either side of station 174, the two cells were relatively homogeneous too. The southern cell was also identified on moored ADCP data by the east (north) velocity intermediate minimum (maximum) in late March (Figure 10a (Figure 10b)). Between the upper layer and the two cells the shear was locally intense, as observed on shipboard ADCP (Figure 2f and Figure 11), moored ADCP (Figures 10a and 10b) and geostrophic current (Figure 9a) data sets. The passage of 96-1 on mooring 7 was marked by strong horizontal currents down to 500 m (up to 30 cm s^{-1}, Figures 10a–10b; increase also clearly recorded on the 1700 m current meter, not shown). Factory algorithms also yielded strong downward velocity, however their validity is currently being investigated. The echo signal (Figure 10c) showed minimum values during the 96-1 passage in the deeper layer (~350–500 m), whereas it corresponded to a maximum in the upper one (~100–300 m).

[21] The chlorophyll distribution (Figure 9c) was also organized in three parts, a major maximum overlying two secondary ones. From the surface down to ~100 m, and reaching almost 150 m in the central zone, chlorophyll concentrations were $\geq$0.75 mg m^{-3} (ec: 0.75 mg m^{-3} at 100 m at station 171). Maximum concentrations were >1.2 mg m^{-3} at ~20–50 m. The thermostad was also identified by localized vertical maximum oxygen concentrations (Figure 9c) reaching ~150 m. The major chlorophyll maximum lower limit was sharp and matched the base of the mixed layer. The same feature applied to dissolved oxygen and light transmission (not shown). Underneath, the two secondary chlorophyll maxima were mirrored by the oxygen distribution. The southern one was well defined between ~130–230 m, with sharp limits at stations 169 and 173. Concentrations were >0.8 mg m^{-3}, as confirmed by the bottle sample: at 150 m at station 171, ec was 0.84 mg m^{-3}, and chlorophyll *a* alone 0.44 mg m^{-3}. The chlorophyll distribution in the northern cell did not exhibit sharp limits, concentrations were homogeneously lower (~0.3 mg m^{-3}).

[22] The transect 136–144 (Figure 12) also cut the southwestern part of 96-1 (station 136 $\approx$ station 171) before the wind event (on 24 March). It showed that a warmer

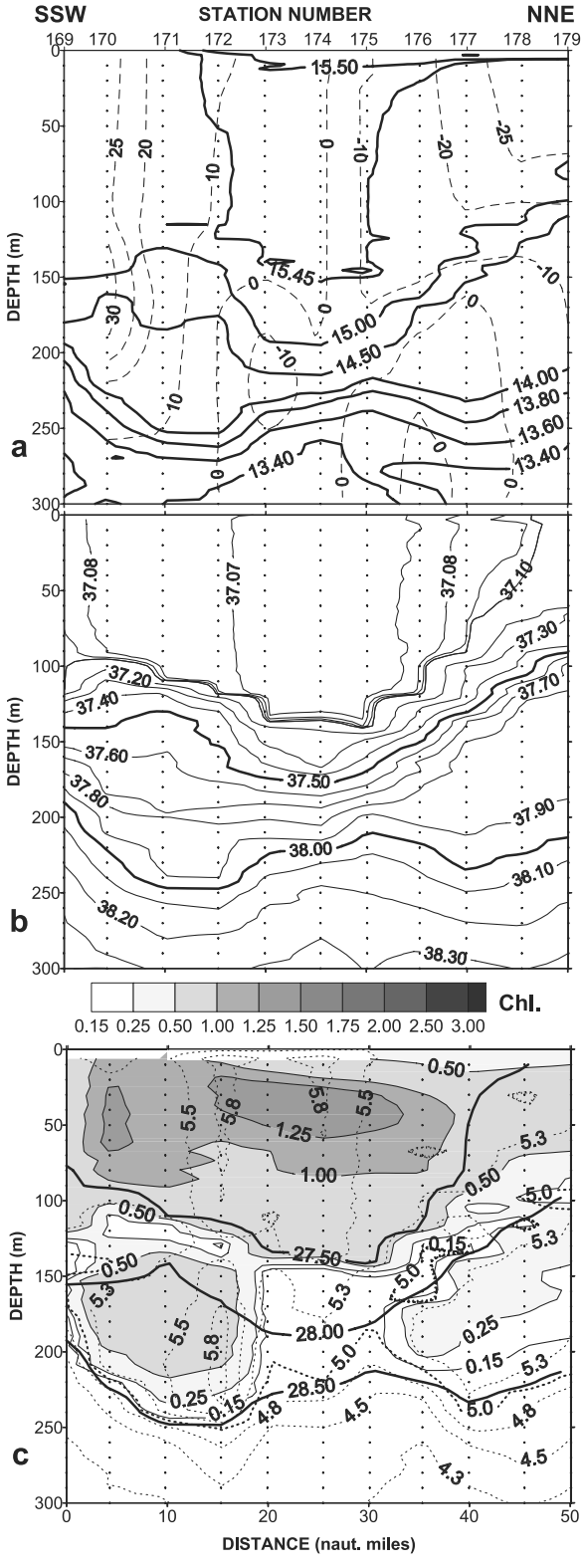

Figure 9. Transect 169–179 inside 96-1 (spring 1998) (a) potential temperature (°C) and geostrophic current (dotted line), (b) salinity, and (c) chlorophyll concentration (mg m^{-3}), potential density (thick solid line), and dissolved oxygen concentrations (relative units, dotted line).

surface layer (>15.50°C) ~20-m-thick capped 96-1 and that chlorophyll was distributed from the surface down to ~80 m, a few patches only reaching 1 mg m^{-3}. There was no secondary deeper maximum.

3.2. AE 97-1

3.2.1. Spring 1998 Conditions (ELISA-3)

[23] AE 97-1 was propagating eastward along the slope (Figures 4b and 4c). Its diameter was ~150 km. The warmer AW signature (Figures 2e–2f) could be tracked from the "reservoir" upstream and offshore around 97-1 up to its eastern side, a part reaching the western edge of 96-1 (filament f3). Because of time constraints only the periph-

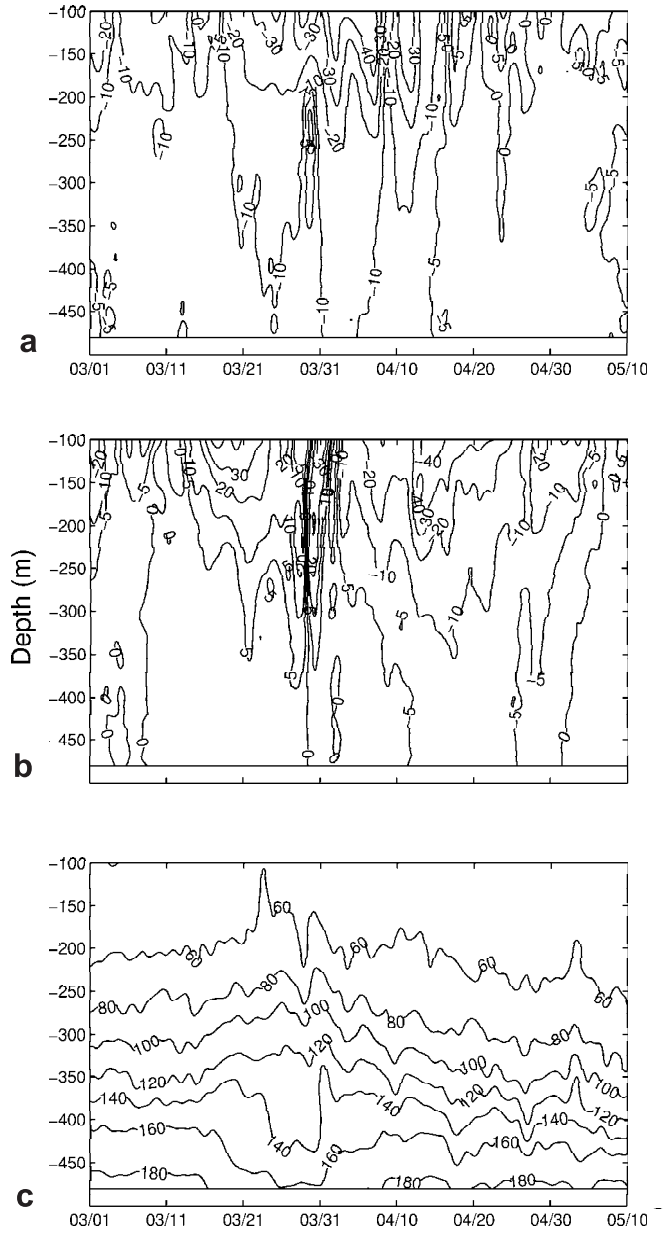

Figure 10. ADCP record of 96-1 passage over mooring 7, from 1 March to 10 May 1998: (a) east velocity component (cm s^{-1}), (b) north velocity component (cm s^{-1}), and (c) echo intensity (counts). See color version of this figure at back of this issue.

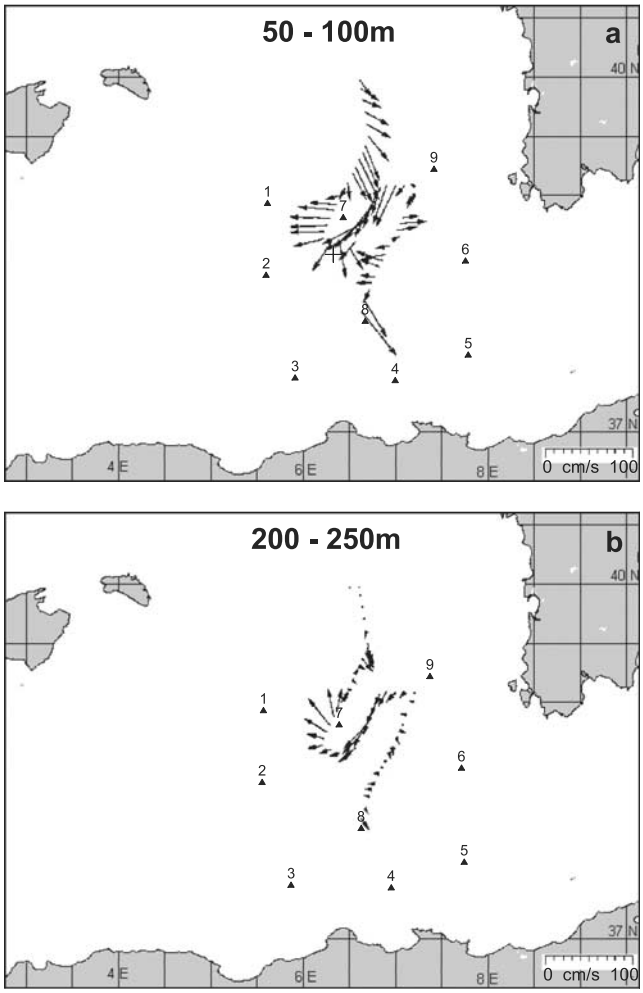

Figure 11. Shipboard ADCP currents measured in 96-1 from 26 to 28 March 1998 (a) in the layer 50–100 m and (b) in the layer 200–250 m.

eral zone was sampled. The Algerian Current was identified on shipboard ADCP currents by maxima of 70–80 cm s^{-1} in the 16–50 m layer (Figure 2f; still significant at 400 m, not shown). Geostrophic current (not shown since the transect was not perpendicular to the current direction) also displayed a distinct superficial core of current ~10–20 miles NNW from station 144, a further observation coherent with the idea of 97-1 being embedded in a meander of the Algerian Current. The transition out of the ensemble Algerian Current-97-1 was very sharp: at only ~10 miles NE of station 144 the current was perpendicular and approximately four times weaker (Figure 2f), in agreement with the sharp thermal signature. The water column was thermally stratified at the 97-1 innermost station (station 144, Figure 12), although weakly. Surface temperature was >16.00°C on the ~30 upper m (less than 15.50°C in 96-1), corresponding to a little modified AW layer of salinity <36.90. The chlorophyll distribution was strictly limited to a well-defined subsurface maximum between 40 and 80 m (maximum ~1.4 mg m^{-3}).

3.2.2. Summer 1998 Conditions (ELISA-4)

[24] AE 97-1 had left the Algerian slope and was offshore, drifting westward (Figure 4d). We made a prelimi-

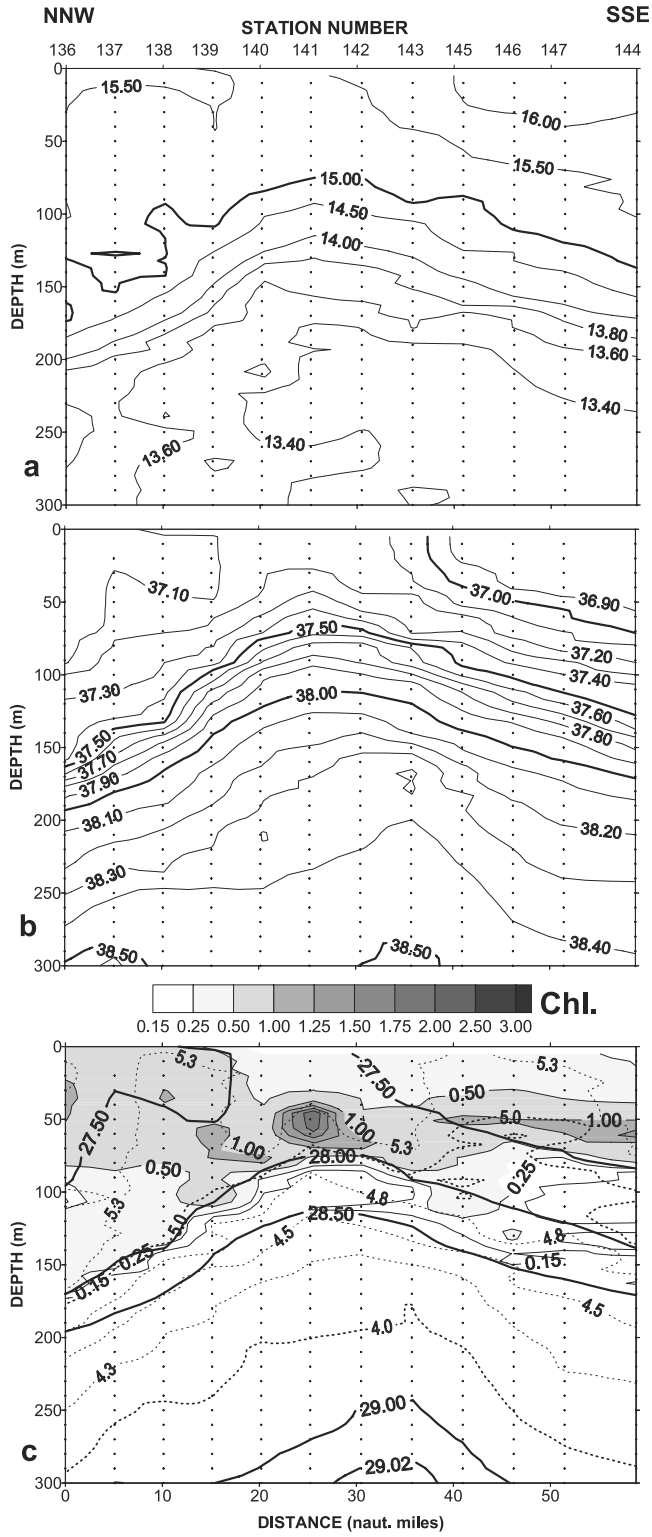

Figure 12. Transect 136–144 from 96-1 to 97-1 (spring 1998): (a) potential temperature (°C), (b) salinity, and (c) chlorophyll concentration (mg m^{-3}), potential density (thick solid line), and dissolved oxygen concentrations (relative units, dotted line).

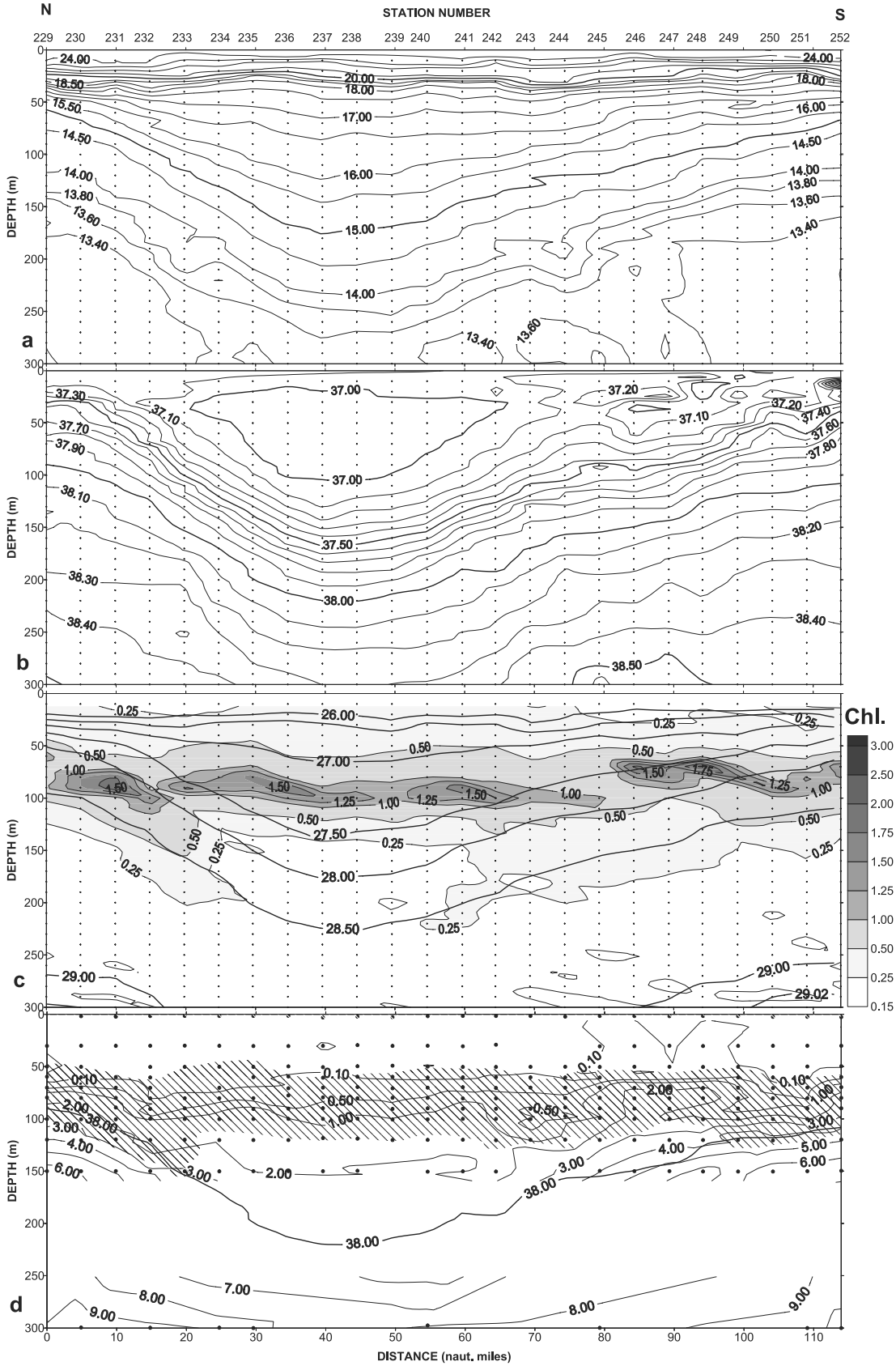

Figure 13. Transect 229–252 across 97-1 (summer 1998) (a) potential temperature (°C), (b) salinity, (c) chlorophyll concentration (mg m^{-3}) and potential density (thick solid line), and (d) nitrate concentration (μM); isohaline 38.00 (thick solid line), and chlorophyll >0.5 mg m^{-3} (cross-hatched).

nary EW transect with XBTs to locate the central zone, and thus precisely positioned the NS transect 229–252 (Figure 13) along a diameter (~180 km). This transect was carried out within 2 days (3–4 July). The center of 97-1 was located in the vicinity of stations 237–238, its northern edge was shortly after station 229 (Figure 5c), and its southern edge was indicated by the shipboard ADCP current speed (Figure 2h) discontinuity at ~38°N, i.e., in the vicinity of stations 246–247. This speed minimum was related to mesoscale interactions: 98-2 altered the eastward along-slope propagation of AW (interactions were even more dramatic a few days earlier [see *Puillat et al.*, 2002]), part of which was entrained back westward around the 97-1 southern edge. This accounted for the southern geostrophic current relative maximum at stations 247–248 (Figure 5c) and for the asymmetry of both the satellite signature (Figure 2g) and sections (Figure 13). Geostrophic currents displayed maxima of 25–40 cm s^{-1} in the upper ~50 m (slightly less and shallower than in 96-1 during the previous summer). Shipboard ADCP currents reached maximum values of 60–70 cm s^{-1} (Figure 2h). In 97-1, the hydrological structure was depressed by ~130 m (Figure 13), however doming of the central surface layer was hardly significant (≤10 m). The striking feature was the isolated homogeneous low-salinity AW core (minimum ~36.92) between ~20 and ~80 m (Figure 13b), overlaid with a continuous saltier layer. Thermal stratification (Figure 13a) was well established from the surface (maximum ~24°C) all the way through the salinity homogenous layer and below.

[25] At mesoscale, chlorophyll (Figure 13c) was distributed in a DCM between 50 and 100 m. The central zone maximum concentrations were 1.0–1.2 mg m^{-3}, up to 1.5 mg m^{-3} at 80–90 m (shallower and larger than in 96-1 during the previous summer). On the offshore peripheral zone they were >2 mg m^{-3} at 80 m. Shoreward, the DCM was slightly shallower (60–80 m), ranging from 1.0–1.3 to 1.8 mg m^{-3}. Slight discontinuities between stations 232–233 and 245–246 separated the DCM of the central zone from the shallower maxima of the peripheral zones (station 231 and stations 246–248). Peripheral DCM signatures were progressively subsiding centerward along isopycnals, down to ~200 m. This was well observed between stations 230 and 233, less on the southern edge on this transect but extremely well marked on the eastern parallel transect (not shown). The surface layer showed low but significant concentrations: ~0.2 mg m^{-3} at ~5 m over the whole transect length. The DCM trailed the nitracline (Figure 13d) in the central zone, but was underneath in the peripheral zone. The nitracline was mostly horizontal, at ~80 m. Below, down to ~150 m at least, the central zone was characterized by low concentrations between 1.0 and 2.0 μM. At 300 m concentrations were >7.0 μM. Nutrient sampling did not allow us to reliably track the correlation between isohaline 38.00 and isopleths 2.0–3.0 μM in the central zone. Both peripheral zones were marked by strong gradients, and at 300 m, nitrate concentrations were >9.0 μM, up to ~10.0 μM at station 252. On the offshore end, the 38.00 isohaline shoaled at ~100 m and corresponded to nitrate concentrations of 2.0–3.0 μM. On the shoreward end, the 38.00 isohaline also roughly shoaled at 100 m and corresponded to the 4.0-μM isopleth (also observed on transect 253–269, not shown).

4. Secondary Eddy-Induced Phenomena

4.1. Small Cyclonic Shear Eddy

[26] Small cyclonic shear eddies (a few tens of km in diameter) are often created by AEs at coastline breaks. As such structures do not last for long (few days to a few weeks) and move as they are advected around AEs, they are more difficult to sample. One was detected during ELISA-1 on the image of 27 July as a colder spot ("C", Figure 2a), ~30–40 km in diameter. Transect 93–99 was performed slightly east of the C center, in a NNE-SSW chord on 28–29 July. Shipboard ADCP currents recorded the cyclonic rotation (Figure 2b) in the upper 100 m. Deep geostrophic currents were not reliable, as the 1000-m profiles were too few. However, in the upper 200 m (not shown) they clearly depicted the cyclonic rotation, the current direction shifting between stations 98 and 97. The hydrological sections (Figures 14a–14c) displayed the typical doming of cyclonic eddies between stations 98 and 96. The doming amplitude was 30–40 m in the central zone, and still significant (~20 m) at 300 m. The C structure was asymmetrical, the isolines slope being steeper toward station 93 because of 96-1. The chlorophyll distribution (Figure 14c) displayed a surface depleted layer, and a DCM significantly shallower (~40–80 m) than in the summer AEs' transects. The largest fluorescence peaks were recorded during the stations 96 and 99 downcast profiles: ~4 mg m^{-3} at ~75 m at station 96, and >8 mg m^{-3} at ~80 m at station 99. The ec (chlorophyll *a*) underestimated maximum was 4.4 mg m^{-3} (2.5 mg m^{-3}) at 70 m at station 96 and 1.9 mg m^{-3} (0.9 mg m^{-3}) at 80 m at station 99. Concentrations rapidly decreased below the DCM (none > 0.5 mg m^{-3} below 90 m). Nitrate distribution (Figure 14d), also doming at station 97, showed significant concentrations in the upper layer, as the nutricline shoaled at ~50 m, mostly above the DCM. The 1.0 μM reached ~50 m in the center, when it was deeper than 100 m in 96-1, hardly reaching 100 m in the peripheral zone. Concentrations at 300 m were ~9.5 μM over the whole transect.

4.2. Shear Zones and Filaments

[27] During spring 1998, 96-1 and 97-1 were close. They induced opposite currents over a short distance, a shear zone resulting in between. Shipboard ADCP currents and rough geostrophic calculations (not shown) indicated that the maximum shear zone was located between stations 141 and 142 (Figure 12). Cutting through two anticyclonic eddies yielded an overall doming hydrological structure: at station 141 the 15.00°C isotherm shoaled up to ~80 m. In this area of high shear there was a pronounced and very localized maximum of ~2.4 mg m^{-3} at 40–50 m at station 141. The same feature was observed on the analogous SW-NE transect (not shown, see location on Figure 4b) from station 144 back to 96-1 (>1.5 mg m^{-3} at 60–80 m). During summer 1998 in the same way, the westward transect between 96-1 and 97-1 (Figure 4d) showed chlorophyll maxima up to 3 mg m^{-3} between 70–100 m.

[28] Filaments are recurrent features associated with AEs. For instance, subsurface salinity maxima and relative temperature maxima at ~100 m at stations 24 and 34 (Figure 6)

revealed that filaments were being advected inside 96-1. Other filaments in 96-1 were indicated by submesoscale hydrological patchiness (as for instance at station 105 and station 114, Figure 7), down to ~300 m at least in the peripheral zone. Some chlorophyll patchiness trailed the filament hydrological variability: for instance the maximum at station 105 (>1.8 mg m^{-3}) was related to a higher-temperature/higher-salinity filament. However, there was no simple relation. The colder filament f1 detected on SST (Figure 2b) was sampled at station 114 but did not exhibit any particular biological signature (Figures 7c–7d) as it was dragging offshore superficial depleted waters. The same observation was made for the filament f2 (Figure 2e) sampled during ELISA-3 (not shown).

[29] The chlorophyll submesoscale spatial variability, related or not to filaments, was a recurrent feature. It could be important, as shown for instance by the isolated 2 mg m^{-3} at station 34 (Figure 6c): only 8–10 km away on both next stations concentrations hardly reached ~0.6 mg m^{-3}.

5. Discussion: Consequences on Mesoscale and Seasonal Scales

5.1. Consequences on Mesoscale

[30] On the mesoscale, the central zones of 96-1 and 97-1, where the depression caused by the anticyclonic motion was 140–160 and 100–120 m, respectively, corresponded to marked oligotrophic areas during summertime. This is illustrated by the difference between the integrated nitrate concentrations (Figure 15) in and out of AEs. The 100-m-integrated nitrate concentration in 97-1 during ELISA-4 (Figure 15c, ~50 mmol m^{-2}) was significantly lower than in the coastal zone (100–200 mmol m^{-2}), where the Algerian Current was flowing and where intense mesoscale interactions occurred, especially with 97-1 and 98-2. During ELISA-1, however, concentrations in 96-1 and out were quasi-homogeneously low (Figure 15a, <100 mmol m^{-2}). Indeed, the absence of low salinities in the southwest of 96-1 confirmed that the Algerian Current was not flowing eastward along slope by then, as it was diverted upstream by 97-1 and then relayed offshore by 96-1. In agreement with this SST-deduced circulation, shipboard ADCP data showed strong westward currents in the south of 96-1 and weak shoreward currents inshore (Figure 2b). As a result 96-1 was surrounded by surface nutrient-depleted water (~50 mmol m^{-2}). On the other hand the difference between AEs and their surroundings was striking on the 200-m-integrated figures (Figures 15b–15d). Minima were encountered in AEs' central zones (200–250 mmol m^{-2} in 96-1 and 250–500 mmol m^{-2} in 97-1), but values increased significantly in the peripheral zones (~500–750 mmol m^{-2}). However, the maximum increase occurred in the coastal and shear zones. In 96-1 during ELISA-1 the integrated chlorophyll concentrations over 200 m (Figure 16a) were

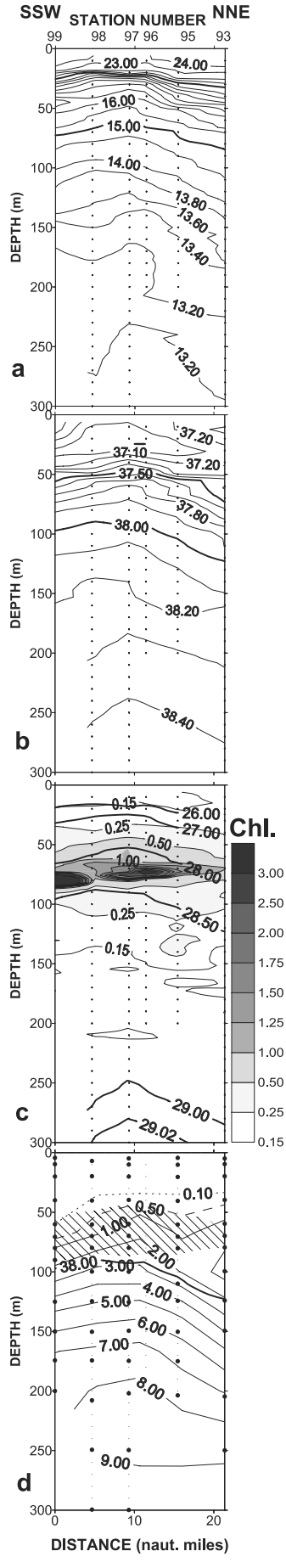

Figure 14. (opposite) Transect 93–99 across C: (a) potential temperature (°C), (b) salinity, (c) chlorophyll concentration (mg m^{-3}) and potential density (thick solid line), and (d) nitrate concentration (μM); isohaline 38.00 (thick solid line), and chlorophyll >0.5 mg m^{-3} (cross-hatched).

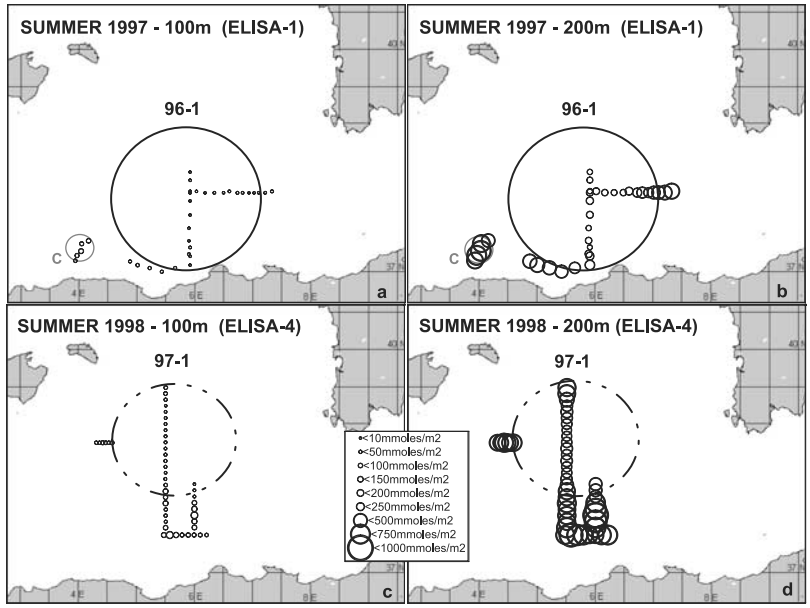

Figure 15. Integrated nitrate in 96-1 during summer 1997 (a) over 100 m and (b) over 200 m and in 97-1 during summer 1998 (c) over 100 m and (d) over 200 m.

homogeneously weak ($\leq$80 mg m^2 but for one maximum, see later in the text). In 97-1 during ELISA-4 the integrated chlorophyll concentrations over 200 m (not shown) were $\sim$100 mg m^2 and 100–140 mg m^2 outside. Because nitrate concentrations were low in the AEs over a layer $\sim$200 m thick, primary production was expected to be low too. Results for ELISA-1 [*Moutin et al.*, 1999; ELISA unpublished data] confirmed that in 96-1 the new production was homogeneously low, and that the primary production was extremely low, in the lower range of values found offshore in the western Mediterranean, even in the lower range of values commonly accepted in the eastern Mediterranean. While neither 96-1 nor 97-1 was under strong and direct influence of the Algerian Current, it must be pointed out additionally that the former, although it was along slope, showed oligotrophic features more pronounced than the latter, which was offshore.

[31] On the AEs' periphery, the downward entrainment of chlorophyll along isopycnals [see, e.g., *Claustre et al.*, 1994] has been clearly shown during summertime (Figures 6c, 7c, and 13c). This convergence occurs in the vicinity of the DCM interruption: for instance on stations 24 and 32 in 96-1 and stations 232–233 and 245–246 in 97-1. Below, the fluorescence signal can be detected down to 200–250 m. This downward entrainment has been well described by the tow-yo transects performed during ELISA-1 down to $\sim$300 m on the 96-1 western and southern sides (not shown). As this movement must be counterbalanced somehow [e.g., *Zakardjian and Prieur*, 1998], one can imagine that the balancing upward motion is achieved by the shoaling, at $\sim$100 m, of the 38.00 isohaline and of higher nitrate ($\sim$1–3 μM) and chlorophyll ($\geq$1 mg m^2) concentrations further toward the edge.

[32] Further mesoscale variability was induced by the secondary phenomena that AEs generate. The enrichment linked to the cyclonic shear eddy was clearly signed: in C were found the maximum chlorophyll concentrations (4–8 mg m^{-3}) of all ELISA cruises (307 CTD casts), and the maxima of the 200-m-integrated nitrate ($\sim$750 mmol m^2, Figure 15b) and chlorophyll ($\sim$110 mg m^2, Figure 16a) concentrations of the ELISA-1 cruise. However, such values are likely to be in a lower range, as the doming due to the cyclonic rotation occurred in severely nutrient-depleted waters (the nutricline was $\sim$80 m deep along the coastal transect south of 96-1; not shown). Zones of shear between an AE and the Algerian Current or between AEs also have a clear biological signature. The maximum integrated nitrate values ($\sim$1000 mmol m^2 over 200 m, Figure 15d), as well as the maximum integrated chlorophyll ones ($\sim$140 mg m^2, not shown), were found in the area where complex interactions occurred between the Algerian Current and AEs 97-1 and 98-2 (ELISA-4). In the same way, the maximum chlorophyll concentrations of ELISA-3 (station 141, $\sim$2.4 mg m^2, Figure 12c) were found in the shear area between 96-1 and 97-1. The consequences of the filaments entrained by the AEs were variable. A thin filament ($\sim$20 m thick) of lower salinity ($\sim$36.95) was responsible for the isolated maximum of integrated chlorophyll ($\sim$100 mg m^2, Figure 16a) close to the 96-1 center. On the other hand, most of the observed filaments drag

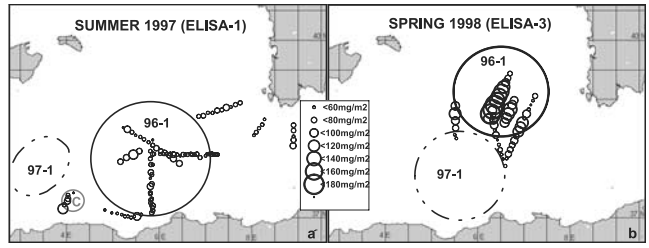

Figure 16. Integrated chlorophyll over 200 m in 96-1 (a) during summer 1997 and (b) during spring 1998.

superficial depleted water (such as f1, Figure 7, and f2, not shown), and have no specific signature.

5.2. Consequences on Seasonal Scale

[33] On the seasonal scale the biological signature of 96-1 changed dramatically between summer and spring, when it was offshore. Mixing was the major feature controlling the 96-1 situation in spring. Since the stratification within 96-1 was already relatively weak in summer (thermostad ~100 m thick beneath the thermocline), it did not require numerous nor strong wind events to trigger mixing, and hence replenish the surface layer with nutrients. A further argument is its doming hydrological structure observed in summer 1997 (Figure 6) which can be legitimately related to mixing, as we know that 96-1 was offshore at least during springtime 1996 [*Puillat et al.*, 2002] (note that the doming feature was not significant in 97-1, which remained stratified throughout wintertime, see below). The presence of phytoplankton down to ~150 m in the 96-1 central zone, as well as the relatively low concentrations encountered (maximum ~1 mg m^{-3}) can be interpreted as resulting from the water column instability and mixing (unfortunately we have no coincident nutrient concentrations or primary production data). High chlorophyll values in the subsurface water cells cannot be explained by local production (>100 m in springtime light conditions). The sharp discontinuity (in both hydrological and biological parameters) between the above major and the underneath secondary chlorophyll maxima indicates that the latter do not have the same origin and/or instantaneous cause as the former, and favors a (rapid) downward movement along isopycnals from the edges centerward. Further elements to promote the role (1) of mixing in the major chlorophyll maximum distribution and (2) of subsidence for the secondary ones are the facts that, prior to the wind event, the chlorophyll maximum was neither so thick nor so deep, and that no secondary chlorophyll maximum was observed on the 96-1 southern periphery (Figure 12). AE 96-1 was clearly identified by the highest 200-m-integrated chlorophyll values (up to 180 mg m^2, Figure 16b), as corroborated by the larger ADCP echo in the upper 200 m (Figure 10c). These observations are consistent with those made in an open sea anticyclonic eddy in the eastern Mediterranean in February-March [*Krom et al.*, 1992; *Zohary et al.*, 1999]. This eddy had undergone deep winter mixing, and the maximum integrated chlorophyll values were observed inside it. The phytoplankton bloom began shortly after the nutrient input by winter mixing, whereas in the Gulf Stream warm core rings the onset of the thermal stratification is necessary. On the other hand, in the peripheral zone of 97-1, which was along slope, values were clearly in the same range as summer values, and corresponded to the minima for ELISA-3 (~60 mg m^2, Figure 16b). Indeed, 97-1 was still embedded in a meander of the Algerian Current, and the thermal stratification had not been destroyed during winter. As a consequence, 97-1 displayed early summer characteristics: weak thermal stratification and shallow subsurface chlorophyll maximum (Figure 12). The observation that open sea isolated eddies can be the richest areas of the eastern Algerian Basin in late winter to early spring receives confirmation from an ocean color satellite image (MOS, Figure 17) acquired one month before (28 February 1998). Both thermal and biological signatures were very much alike, which highlights the importance of mesoscale dynamics for biological phenomena in the Algerian Basin. The two AEs in the center of the basin (98-1 and the one north of it) corresponded to the highest chlorophyll concentrations (besides the northern part of the basin). Concentrations in the coastal AE were definitely lower, even though it generated locally intense maxima along the coastline (red patch). Such AEs thus represent less favorable conditions for phytoplankton blooms at that time than open sea ones. However, this "spring" period requires further investigation, as the CTDFs time series (not shown) indicate that the chlorophyll maximum values of the yearlong records occurred between late December and mid-February, without any strong mesoscale dynamical signal.

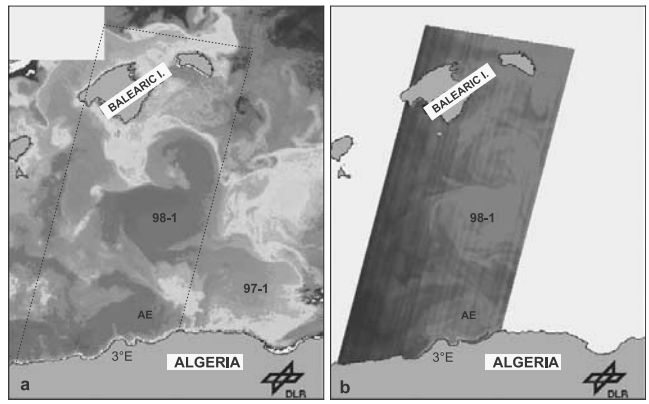

Figure 17. Satellite images of 28 February 1998. (a) NOAA/AVHRR image; temperature increases from blue to red. (b) Modular Optoelectronic Scanner (MOS) image: algal pigment distribution; concentration increases from deep blue to green, up to red. MOS image provided by DLR/Institute of Space Sensor Technology. See color version of this figure at back of this issue.

6. Conclusion: Perspectives on Consequences on Basin Scale

[34] It appears that the variability of AEs is so important that it precludes, for now, any relevant comparison with other rings and eddies. Because AEs are anticyclonic, and can have diameters up to ~200 km, they represent less favorable conditions for biological growth, especially during the long stratified period. On a yearly average, however, AEs at the coast are more likely to induce enrichment processes. In the western part of the basin they develop upwellings, and often shallow cyclonic circulations as well, that represent enriched areas [*Moran et al.*, 2001]. They can also interact with the Algerian Current, and/or with coastline breaks, all of these being associated with higher biological signals, as seen in the shoreward ends of the 97-1 summer transects. This is confirmed by yearly averages of CZCS-derived pigments and primary production [e.g., *Antoine et al.*, 1995, see Plate 4], showing a more productive strip along the Algerian coast. The fact that this strip begins in the vicinity of 0° (point where the Almeria-Oran Jet becomes the Algerian Current) and stops in the vicinity of 9°E (where AEs leave the coast because

of bathymetry) clearly involves the Algerian Current instability (all the more since there is no continental shelf). The front it delimits in the western part is related to a phytoplankton biomass increase [*Lohrenz et al.*, 1988b; *Raimbault et al.*, 1993]. On the other hand, the ELISA data show that the Algerian Current instability can also lead to most oligotrophic areas in the coastal zone, when old AEs come back in the coastal zone.

[35] However, we have seen that the AEs offshore during wintertime and springtime might represent large areas of enhanced biological activity. Since the subsurface homogeneous layer was observed in both 96-1 and 97-1, as well as in a previous AE transect [*Benzohra and Millot*, 1995b], and since the general counterclockwise circuit brings AEs offshore, conditions for mixing and strong vertical velocities (and subsequent phytoplankton blooms) are likely to occur offshore a few times per year. Moreover, the generation of shear zones and of small cyclonic shear eddies might dampen the unfavorable effect of anticyclones. We have observed in the AEs' peripheral zone the shoaling ($\sim$100 m) of the 38.00 isohaline, generally associated with nitrate concentrations of 2–3 μM (that is, similar to what is observed at $\sim$200–250 m, as in the AEs' central zones). This nitrate (and phosphate, not shown) input into the euphotic layer was marked by higher chlorophyll concentrations. This means that, thanks to mesoscale dynamical activity, Mediterranean water (salinity >38.00) can locally contribute to production, even in the open basin. For all the aforementioned processes, the question is then to determine whether these contributions, although spatially and temporally limited, are significant on a yearly basis and on a basin scale.

[36] However it is legitimate to hypothesize that AEs are key elements in the transfer of matter on basin scale [see *Gorsky et al.*, 2002]. First, the AEs, that represent large volumes, drift in the Algerian Basin and release water when they disappear. Second, they induce numerous horizontal movements with filaments. However, although such filaments can be very long (f1 $\sim$250–300 km) and last for relatively long periods (f1: >4 weeks), most of them appear to be very thin (10–20 m thick). Since the upper layer of AEs remains isolated to some extent, as shown by the distinct cores of lower salinity in long-lived (offshore) AEs, filaments are most likely to have a limited impact. Last, AEs induce vertical movements all yearlong on their periphery (downward entrainment along isopycnals and potential counterbalancing upward movement), and temporally in their central zone offshore (mean downward velocity, and sporadic subsidence). All these processes might combine to reduce the overall oligotrophy of the open Algerian Basin.

[37] It appears that, even with a sampling scheme allowing for a fine-scale description over a long period of time, the variability of AEs is so important, depending on their history, age, season, location, and dynamical environment, that these observations do not allow us to reliably assess their impact at basin scale, or to propose a definitive scheme of functioning yet.

[38] **Acknowledgments.** The collaboration of the German aerospace center DLR has been a cornerstone of the ELISA strategy, and the DLR team is warmly thanked. The collaboration with J. Font (ICM-CSIC Barcelona) increased the number of currentmeters deployed. We are grateful to C. Albérola, G. Coustillier, M. Emelianov, C. Fernandez, J.-L. Fuda, N. Garcia, B. Rey, S. Ruiz, and J. Sudre for help in data acquisition and processing, as well as to members of DT INSU in Brest and La Seyne for help with instruments and ships logistics. Warmest thanks are extended to crewmembers and fleet administrators for having dealt with real-time sampling schemes. Support for ELISA was provided by EEC, IFREMER and INSU/CNRS, and I. Puillat was supported by a DRET/DGA fellowship. Contribution MTP II-MATER/042.

References

Aiken, J., A. Gargett, C. Marrase, B. Rothschild, and I. Taupier-Letage, Regional studies: Small to sub-basin scales, in *Report of the First Meeting of the International GLOBEC Working Group on Sampling and Observation Systems*, *GLOBEC Rep. 3*, pp. 41–51, Intergov. Oceanogr. Comm., U. N. Educ., Sci., and Cult. Org., Paris, 1993.

Antoine, D., A. Morel, and J. M. André, Algal pigment distribution and primary production in the eastern Mediterranean as derived from Coastal Zone Color Scanner observations, *J. Geophys. Res.*, *100*, 16,193–16,209, 1995.

Arnone, R. A., and La Violette, Satellite definition of the bio-optical and thermal variation of coastal eddies associated with the African Current, *J. Geophys. Res.*, *91*, 2351–2364, 1986.

Arnone, R. A., D. A. Wiesenburg, and K. D. Saunders, The origin and characteristics of the Algerian Current, *J. Geophys. Res.*, *95*, 1587–1598, 1990.

Benzohra, M., and C. Millot, Characteristics and circulation of the surface and intermediate water masses off Algeria, *Deep Sea Res., Part I*, *42*, 1803–1830, 1995a.

Benzohra, M., and C. Millot, Hydrodynamics of an open sea Algerian Eddy, *Deep Sea Res., Part I*, *42*, 1831–1847, 1995b.

Claustre, H., P. Kerherve, J.-C. Marty, and L. Prieur, Phytoplankton photoadaptation related to some frontal physical processes, *J. Mar. Syst.*, *5*, 251–265, 1994.

ELISA Group, ELISA: Eddies and Leddies Interdisciplinary Study in the Algerian Basin, *MTP News*, *6*, 9–10, 1998.

Font, J., C. Millot, J. Salas, A. Julia, and O. Chic, The drift of Modified Atlantic Water from the Alboran Sea to the eastern Mediterranean, *Sci. Mar.*, *62*, 211–216, 1998.

Fuda, J.-L., C. Millot, I. Taupier-Letage, U. Send, and J. M. Bocognano, XBT monitoring of a meridian section across the western Mediterranean Sea, *Deep Sea Res., Part I*, *47*, 2191–2218, 2000.

Gorsky, G., L. Prieur, I. Taupier-Letage, L. Stemmann, and M. Picheral, Large particulate matter in the western Mediterranean; I, LPM distribution related to mesoscale hydrodynamics, *J. Mar. Syst.*, 33–34, 289–311, 2002.

Herbland, A., A. Le Bouteiller, and P. Raimbault, Size structure of phytoplankton in the equatorial Atlantic Ocean, *Deep Sea Res., Part A*, *32*, 819–836, 1985.

Kirkwood, D. S., Stability of solutions of nutrient salts during storage, *Mar. Chem.*, *38*, 151–164, 1992.

Krom, M. D., S. Brenner, N. Kress, A. Neori, and L. I. Gordon, Nutrient dynamics and new production in a warm-core eddy from the eastern Mediterranean Sea, *Deep Sea Res., Part A*, *39*, 467–480, 1992.

Lohrenz, S. E., R. A. Arnone, D. A. Wiesenburg, and I. P. Depalma, Satellite detection of transient enhanced primary production in the western Mediterranean Sea, *Nature*, *335*, 245–247, 1988a.

Lohrenz, S. E., D. A. Wiesenburg, I. P. Depalma, K. S. Johnson, and D. E. Gustafson Jr., Interrelationships among primary production, chlorophyll, and environmental conditions in frontal regions of the western Mediterranean Sea, *Deep Sea Res., Part A*, *35*(5), 793–810, 1988b.

Martinez, R., R. A. Arnone, and Z. Velasquez, Chlorophyll *a* and respiratory electron transport system activity in microplankton from the surface waters of the western Mediterranean, *J. Geophys. Res.*, *95*, 1615–1622, 1990.

Mediprod-5 Group, Variabilité à moyenne échelle du Bassin Algérien, Observations hydrologiques, biologiques et chimiques, in *GDR P4*, edited by C. Millot and M. C. Bonin, 121 pp., Inst. Fr. de Rech. pour l'Exploit. de la Mer, Brest, France, 1990.

Millot, C., Some features of the Algerian Current, *J. Geophys. Res.*, *90*, 7169–7176, 1985.

Millot, C., The circulation of the Levantine Intermediate Water in the Algerian Basin, *J. Geophys. Res.*, *92*, 8265–8276, 1987.

Millot, C., Mesoscale and seasonal variabilities of the circulation in the western Mediterranean, *Dyn. Atmos. Oceans*, *15*, 179–214, 1991.

Millot, C., Models and data: A synergetic approach in the western Mediterranean sea, in *Ocean Processes in Climate Dynamics: Global and Mediterranean Examples*, edited by P. Malanotte-Rizzoli and A. R. Robinson, pp. 407–425, Kluwer Acad., Norwell, Mass., 1994.

Millot, C., Circulation in the western Mediterranean sea, *J. Mar. Syst.*, *20*, 423–442, 1999.

Millot, C., and I. Taupier-Letage, Additional evidence of LIW entrainment across the Algerian Basin by mesoscale eddies and not by a permanent westward-flowing vein, *Prog. Oceanogr.*, in press, 2003.

Millot, C., I. Taupier-Letage, P. Le Borgne, M. J. Garcia, and L. Wald, Dynamical oceanography studies from infrared remote sensing in the western Mediterranean Sea, in *Mémoires de l'Institut océanographique*, vol. 18, pp. 1–11, Monaco, 1994.

Millot, C., I. Taupier-Letage, and M. Benzohra, Circulation off Algeria inferred from the Médiprod-5 current meters, *Deep Sea Res., Part I*, *44*, 1467–1495, 1997.

Moran, X., I. Taupier-Letage, E. Vasquez-Dominguez, S. Ruiz, L. Arin, P. Raimbault, and M. Estrada, Physical-biological coupling in the Algerian Basin (SW Mediterranean): Influence of mesoscale instabilities on the biomass and production of phytoplankton and bacterioplankton, *Deep Sea Res., Part I*, *48*, 405–437, 2001.

Morel, A., and J. M. André, Pigment distribution and primary production in the western Mediterranean as derived and modeled from Coastal Zone Color Scanner observations, *J. Geophys. Res.*, *96*, 12,685–12,698, 1991.

Moutin, T., P. Raimbault, and J.-C. Poggiale, Primary production in surface waters of the western Mediterranean Sea: Calculation of daily production, *C. R. Acad. Sci. III*, *322*, 651–659, 1999.

Obaton, D., C. Millot, G. C. D'Hières, and I. Taupier-Letage, The Algerian Current: Comparisons between in situ and laboratory measurements, *Deep Sea Res.*, *47*, 2159–2190, 2000.

Puillat, I., I. Taupier-Letage, and C. Millot, Algerian Eddies lifetime can near 3 years, *J. Mar. Syst.*, *31*, 245–259, 2002.

Raimbault, P., M. Rodier, and I. Taupier-Letage, Size fraction of phytoplankton in the Ligurian Sea and the Algerian Basin: Size distribution versus total concentration, *Mar. Microb. Food Webs*, *3*, 1–7, 1988a.

Raimbault, P., I. Taupier-Letage, and M. Rodier, Vertical size distribution of phytoplankton in the western Mediterranean Sea during early summer, *Mar. Ecol. Prog. Ser.*, *45*, 153–158, 1988b.

Raimbault, P., H. Illoul, and I. Taupier-Letage, Description générale de la distribution de la chlorophylle *a*, in *Variabilité à Moyenne Échelle du Bassin Algérien, CNRS GDR P4*, edited by C. Millot and M. C. Bonin, pp. 105–108, Inst. Fr. de Rech. Pour l'Exploit. De la Mer, Brest, 1990a.

Raimbault, P., M. G. Besse, F. Lochet, and T. Nguyen, Description générale des sels nutritifs, in *Variabilité à Moyenne Échelle du Bassin Algérien, CNRS GDR P4*, edited by C. Millot and M. C. Bonin, pp. 100–104, Inst. Fr. de Rech. Pour l'Exploit. De la Mer, Brest, 1990b.

Raimbault, P., B. Coste, M. Boulhadid, and B. Boudjellal, Origin of high phytoplankton concentration in deep chlorophyll maximum (DCM) in a frontal region of the southwestern Mediterranean Sea (Algerian Current), *Deep Sea Res., Part I*, *40*, 791–804, 1993.

Robinson, A. R., (Ed.), *Eddies in Marine Science*, 609 pp., Springer Verlag, New York, 1983.

Ruiz, S., J. Font, M. Emelianov, J. Isern-Fontanet, C. Millot, and I. Taupier-Letage, Deep structure of an open sea eddy in the Algerian Basin, *J. Mar. Syst.*, *33–34*, 179–195, 2002.

Send, U., J. Font, G. Krahmann, C. Millot, M. Rhein, and J. Tintoré, Recent advances in studying the physical oceanography of the western Mediterranean Sea, *Prog. Oceanogr.*, *44*, 37–64, 1999.

Taupier-Letage, I., Biodynamique du Bassin Algérien: Estimation de la réponse biologique à certaines structures moyenne échelle par télédétection (AVHRR et CZCS) et mesures in situ, Ph.D. thesis, 120 pp., Univ. d'Aix-Marseille II, Marseille, France, 1988.

Taupier-Letage, I., and C. Millot, Surface circulation in the Algerian Basin during 1984, *Oceanol. Acta*, *9*, 119–131, 1988.

Taupier-Letage, I., C. Millot, S. Dech, R. Meisner, J. L. Fuda, I. Puillat, C. Begue, B. Rey, and C. Alberola, Suivi des structures dynamiques de mésoéchelle pendant l'opération ELISA (1997–1998) dans le Bassin Algérien par l'imagerie satellitaire thermique NOAA/AVHRR: Les obstacles potentiels à une reconnaissance automatique, *Oceanis*, *24*, 101–122, 1998.

Tréguer, P., and P. Le Corre, *Manuel d'Analyse des Sels Nutritifs Dans l'Eau de Mer: Utilisation de l'AutoAnalyseur II Technicon*, 2nd ed., Univ. Bretagne Occidentale, Brest, France, 1975.

Zakardjian, B., and L. Prieur, Biological and chemical signs of upward motions in permanent geostrophic fronts of the western Mediterranean, *J. Geophys. Res.*, *103*, 27,849–27,866, 1998.

Zohary, T., S. Brenner, M. D. Krom, D. L. Angel, N. Kress, W. K. W. Li, A. Neori, and Y. Z. Yacobi, Buildup of microbial biomass during deep winter mixing in a Mediterranean warm-core eddy, *Mar. Ecol. Prog. Ser.*, *167*, 47–57, 1999.

C. Millot, I. Puillat, and I. Taupier-Letage, Laboratoire d'Océanographie et Biogéochimie (LOB), CNRS UMR 6535, Université de la Méditerranée, Antenne de Toulon, BP 330, F-83507 La Seyne sur Mer, France. (itaupier@ifremer.fr)

P. Raimbault, Laboratoire d'Océanographie et Biogéochimie (LOB), CNRS UMR 6535, Université de la Méditerranée, Campus de Luminy, Case 901, F-13288 Marseille Cedex 09, France.

Figure 2. (opposite) Mesoscale location and sampling sites during the ELISA cruises (only the best time coherent subsets of satellite and in situ observations are presented). Pluses are CTD transects discussed in text, identified by their end station numbers. Solid triangles are moorings. Temperature on NOAA/AVHRR images increases from blue to red. Arrows are shipboard ADCP currents in the 16–50-m layer. (a) ELISA-1 CTD transects over NOAA/AVHRR image of 28 July 1997. (b) ADCP currents from 24 July to 2 August 1997 over NOAA/AVHRR image of 27 July 1997. (c) ELISA-2 CTD transect over NOAA/AVHRR image of 19 October 1997. d) NOAA/AVHRR image of 27 October 1997. (e) ELISA-3 CTD transects over NOAA/AVHRR image of 27 March 1998. (f) ADCP currents from 26 to 28 March 1998, over NOAA/AVHRR image of 27 March 1998. (g) ELISA-4 CTD transect over NOAA/AVHRR image of 6 July 1998. (h) ADCP from 1 to 6 July 1998 over NOAA/AVHRR image of 6 July 1998.

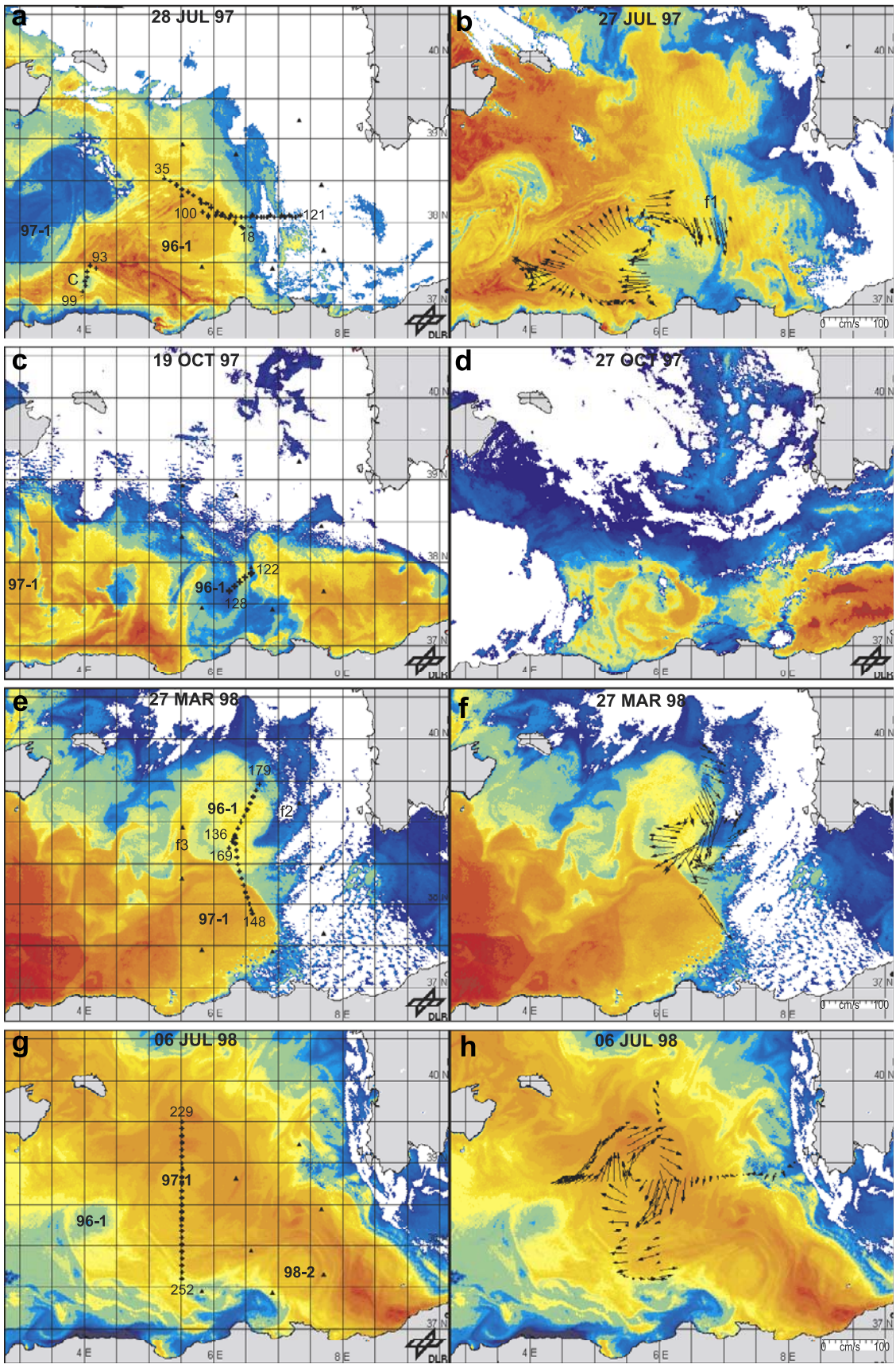
a
28 JUL 97
35
100
121
97-1
18
96-1
93
C
99
b
27 JUL 97
f1
0 cm/s 100
c
19 OCT 97
122
97-1
96-1
128
d
27 OCT 97
e
27 MAR 98
179
96-1
f2
136
f3
169
97-1
148
f
27 MAR 98
0 cm/s 100
g
06 JUL 98
229
97-1
96-1
98-2
252
h
06 JUL 98
0 cm/s 100

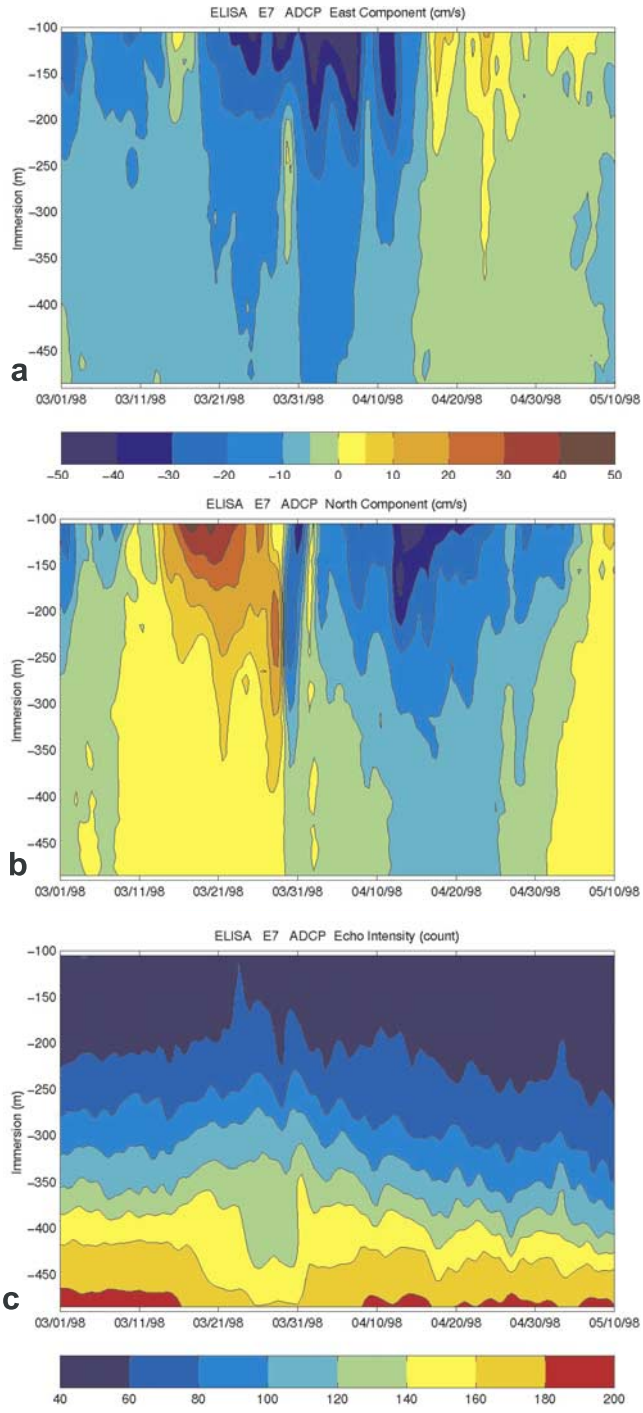

Figure 10. ADCP record of 96-1 passage over mooring 7, from 1 March to 10 May 1998: (a) east velocity component (cm s^{-1}), (b) north velocity component (cm s^{-1}), and (c) echo intensity (counts).

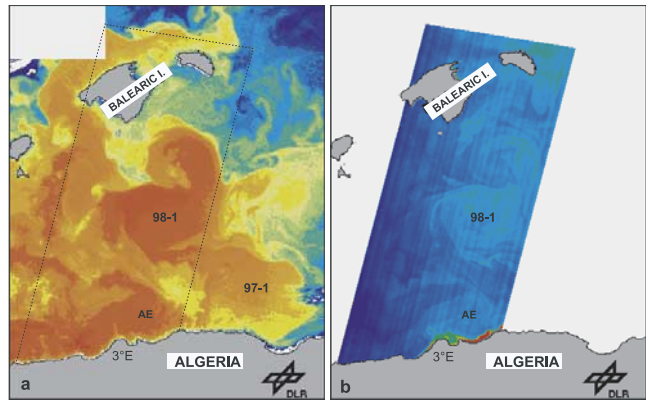

Figure 17. Satellite images of 28 February 1998. (a) NOAA/AVHRR image; temperature increases from blue to red. (b) Modular Optoelectronic Scanner (MOS) image: algal pigment distribution; concentration increases from deep blue to green, up to red. MOS image provided by DLR/Institute of Space Sensor Technology.